

PAPER

# Constant rank factorisations of smooth maps, with applications to sonar

Michael Robinson 

Mathematics and Statistics, American University, Washington, DC 20016, USA  
Email: [michaelr@american.edu](mailto:michaelr@american.edu)

**Received:** 22 February 2022; **Revised:** 25 October 2022; **Accepted:** 30 October 2022;  
**First published online:** 1 December 2022

**Keywords:** Factorization category; smooth map; sonar signal processing

**2020 Mathematics Subject Classification:** 18F60 (Primary); 94A12 (Secondary)

## Abstract

Sonar systems are frequently used to classify objects at a distance by using the structure of the echoes of acoustic waves as a proxy for the object's shape and composition. Traditional synthetic aperture processing is highly effective in solving classification problems when the conditions are favourable but relies on accurate knowledge of the sensor's trajectory relative to the object being measured. This article provides several new theoretical tools that decouple object classification performance from trajectory estimation in synthetic aperture sonar processing. The key insight is that decoupling the trajectory from classification-relevant information involves factoring a function into the composition of two functions. The article presents several new general topological invariants for smooth functions based on their factorisations over function composition. These invariants specialise to the case when a sonar platform trajectory is deformed by a non-small perturbation. The mathematical results exhibited in this article apply well beyond sonar classification problems. This article is written in a way that supports full mathematical generality.

## 1. Introduction

Sonar systems are frequently used to classify objects at a distance by using the structure of the echoes of acoustic waves as a proxy for the object's shape and composition. To obtain good classification accuracy, many sonar systems use a moving sensor platform to produce a *synthetic aperture*. As the sensor platform's position changes, one can measure how the echoes change, and from these changes deduce properties of the object.

Traditional synthetic aperture processing is highly effective in solving classification problems when the conditions are favourable but relies on accurate knowledge of the sensor's trajectory relative to the object being measured. Any deviations from the expected trajectory degrade the classification performance of the overall system. Because of this, there is a well-established practice of *motion compensation* and *autofocus* algorithms that iteratively apply corrections to the estimated trajectory in hopes of removing these deviations.

While the autofocus approach works well for small perturbations of the expected trajectory, it suffers when the initial guess of the trajectory is bad. It is natural to ask, 'can one obtain good classification accuracy from synthetic aperture sonar images *without* a good trajectory estimate?' Given that the signatures (the ensemble of all received echoes) of different targets appear to have quite different geometry and topology [49], classification may be possible even given inaccurate trajectory information.

This article provides several new theoretical tools that decouple object classification performance from trajectory estimation in synthetic aperture sonar processing. It does so by defining several new

general topological invariants for smooth functions, which specialise to the case when a sonar platform's trajectory is deformed by a non-small perturbation.

Although this article is theoretical in nature and does not seek to provide ready-to-use processing algorithms, the decoupling of trajectory from classification performance means that good trajectory information is not necessary for sonar object classification. Indeed, Proposition 11 establishes that the image of the sonar signature – the space of pulse echoes without regard to the order in which they arrive – is the governing factor behind the good classification performance observed in [49].

The mathematical results exhibited in this article apply well beyond sonar classification problems, so this article is written in a way that supports full mathematical generality. The key insight is that decoupling the trajectory from classification-relevant information involves factoring a function into the composition of two functions. Generalising this insight, for a smooth function  $u$  we define two categories **QuasiP**( $u$ ) and **Const**( $u$ ) that describe classes of factorisations of  $u$  by function composition under certain constraints. While the constraints were motivated by the needs of sonar classification, they are sufficiently weak to permit wide usage of these categories.

The plan for the paper is as follows. In the next few subsections, we discuss the literature for synthetic aperture sonar target classification (Section 1.1), which provides context for the contributions of this article (Section 1.2). In Section 2, we introduce the concept of circular synthetic aperture sonar (CSAS) and the specific classification problem to be addressed in the rest of the article. CSAS is widely used to collect information about underwater objects. The interested reader who is unfamiliar with the basics can consult one of the many papers on the topic, for instance [22, 39, 44]. In Section 3, we introduce the factorisation categories **QuasiP**( $u$ ) and **Const**( $u$ ) and prove several fundamental results about them, including a complete characterisation of **QuasiP**( $u$ ) for CSAS. Although this complete characterisation is of limited utility for **Const**( $u$ ), we show that a pair of views of the same target establishes an equivalence between functions using common factors. We develop this idea in Section 4 by defining a category **CRSE**( $u_1, u_2$ ) of factorisation equivalences and ultimately prove a characterisation theorem for this category. The theoretical machinery we have constructed is used to revisit the motivating CSAS example in Sections 3.3 and 4.4. Finally, we provide a brief conclusion in Section 5.

### 1.1. Historical context

The process of forming an image from synthetic aperture sonar data uses a bank of spatial matched filters (pixels) over the region where a sonar target is located. Because sonar targets tend to be spatially localised, high-resolution image-based methods are highly effective at rejecting background clutter. Image-based methods generally require accurate knowledge of the sensor platform's trajectory relative to the object being measured, careful control of the sonar waveform, and intimate knowledge of the clutter environment. Hundreds of papers attest to the effectiveness of image-based methods when the conditions are favourable. As a brief sample, the reader is encouraged to consult [6, 7, 8, 9, 11, 17, 23, 26, 34], though this list is not exhaustive. When information about the sensor platform trajectory is not sufficiently accurate, the recovered energy spreads across neighbouring filters in the image (pixels), leading to blurring. Theoretically, blurring is a manifestation of the instability of the Fourier transform when the domain is deformed [30]. Classification becomes difficult if one is forced to start with blurred images.

Since the sensor platform has inertial mass, it is often possible to determine compensations to the filters to account for its motion. When motion compensations are applied, this results in a more focused image [15]. Moreover, when the trajectory is known to be close to a given trajectory – a circular orbit around the target for instance – then motion compensation can improve object classification [38]. The impacts of motion blurring on classification with and without compensation have been discussed in the literature, for instance [4, 16]. Specific considerations related to motion effects in CSAS systems have also been discussed [38, 40].

Because the *scattering transform* is Lipschitz continuous relative to small deformations [1, 5, 37], it can be used to mitigate small, arbitrary trajectory and propagation distortions in sonar signals [50]. The

scattering transform works by decomposing the signal via local convolutions with wavelets or another frame of localised functions. When the distortions are small, the fact that sonar signals of interest tend to be sparse in this basis can be used to isolate the target's response from the distortions. Robust stability results for many frames commonly in use have been established [54]. However, the scattering transform suffers from the 'curse of dimensionality', which means that it can be rather difficult to determine *a priori* which subspace constitutes the target response. Consequently, the scattering transform can be computationally expensive. This happens because the scattering transform explicitly characterises the distinction between target responses and trajectory distortions. Since the present article explores this distinction implicitly, it provides a perspective on sonar data that is complementary to the scattering transform and may ultimately require less computation.

The fact that classification can sometimes succeed with poor trajectory information suggests that non-image-based methods could succeed as well. Statistical machine learning methods applied to the raw sonar echoes are a natural choice. Indeed, machine learning has been successfully applied to sonar classification problems over the past three decades, going back to the beginnings of the subject [2, 3, 10, 13, 20, 25, 32, 56]. Unfortunately, machine learning requires large and diverse training data sets, which can be expensive to obtain. The implication for sonar classification is that the data need to contain not only the targets of interest, but also enough diversity to capture physical effects due to shadows, background structure and pose [55].

A different perspective is to take the *space of echoes* arising from a given target as a *feature* in the abstract, rather than as a point in some high-dimensional space. Comparing such abstract spaces using *homotopy equivalence* is the dominant technique in the mathematical discipline of algebraic topology. By construction, homotopy equivalence is automatically robust to deformations, so it might seem to be ideally suited for sonar classification problems. Unfortunately homotopy equivalence is neither easily testable nor robust to statistical noise. However, a regularised version of homotopy equivalence, called *persistent homology*, is algorithmically computable and is noise robust. The use of persistent homology to study data sets forms the basis of topological data analysis (TDA), for which a standard classification pipeline has emerged [12, 14, 33].

TDA can be applied to sonar classification by comparing the space of echoes arising from an unknown target with a dictionary of spaces for known targets. The traditional TDA pipeline does not consider the ordering of the pulses, since persistent homology is only sensitive to the relationship between similar echoes. Those pulses that are transmitted from nearby locations will be near one another in the space of echoes and so also will those pulses arising from symmetries in the target. While most sonar targets are unlikely to be actually symmetric, strong spatial Fourier modes can yield the same effect. There is a large literature on signals with strong Fourier modes, which are called *almost periodic* functions.

Unfortunately, homotopy equivalence is not the proper equivalence for sonar targets. Since the standard TDA pipeline cannot discriminate between spaces that are homotopy equivalent, TDA is not strictly applicable to sonar echoes. Specifically, homotopy equivalence is both too weak and too strong! As a brief example of the inappropriateness of homotopy equivalence in sonar, it has been shown that homotopy equivalence spuriously detects the direction that the sensor platform orbits a target in CSAS [45]. Conversely, homotopy equivalence fails to discriminate between the echoes arising from a spherical target and an extended one, such as a rod, since both have contractible spaces of echoes. Nevertheless, persistent homology can yield an effective classifier for sonar targets [49]. Moreover, justification for using the space of echoes is established by Proposition 11.

To obtain a better equivalence, one needs to supply information about the ordering of the pulses. In this case, the object to be classified is not merely the space of echoes, but a function from the trajectory to the space of echoes. There are some TDA tools that look at such functions [19, 27, 52]; these are special cases of what this article presents in Section 3.2.

This article relies on the idea of factoring functions through various manifolds. For the practical usage of factorisations in CSAS, one must factor through a circle. Such factorisations through circles have recently become practical through the moniker of *finding circular coordinates* for data sets using *persistent cohomology*. The interested reader is referred to [18, 36, 42, 43, 53].

At a high level, this article seeks to explore a kind of signal processing that is aware of the underlying topology of the space of echoes. Several kinds of filters that are sensitive to topological features are known [21, 46, 47, 48], though it is clear that the works referenced do not exhaust the possibilities. The results of this article could provide a basis for extending these filters, by supplying the base topological data upon which such filters are built.

## 1.2. Contributions

From a mathematical perspective, the focus of this article is to classify smooth maps  $u : M \rightarrow N$  based on factorisations of  $u$  into the composition of two functions. The article defines two new differential topological invariants for a smooth map  $u$  that are distinct from its homotopy class. These invariants are the categories **Const**( $u$ ) and **QuasiP**( $u$ ) of factorisations of  $u$  (Definition 2). In addition to the factorisation categories for a single map, the article also defines a new differential topological invariant **CRSE**( $u_1, u_2$ ) for a pair of smooth maps  $u_1, u_2$  that relates their respective factorisations to each other (Definition 8). Each isomorphism class of **CRSE**( $u_1, u_2$ ) identifies an individual sonar target that could have yielded both the responses  $u_1$  and  $u_2$  under different conditions.

From a practical perspective, the three new invariants allow one to deduce whether changes in sensor configuration or trajectory might be able to confound two objects within a CSAS collection. (Unfortunately, we have not discovered an efficient way to compute these invariants in all cases, though **QuasiP**( $u$ ) can be computed algorithmically in the case of CSAS using Theorem 2.)

As already noted, [49] shows that persistent homology can be used to classify targets without image formation. But why should a topological invariant (homology) be useful in classification? Proposition 11 establishes a sufficient condition for homology of the space of echoes to be an effective solution. Moreover, Theorem 2 provides a more complete answer to this question by establishing that the **QuasiP**( $u$ ) of a CSAS signature is determined by the fundamental group (a topological property), and this is preserved if the trajectory is deformed. This is still only a partial answer for two reasons: (1) not only topology but also geometry impacts persistent homology, and (2) many realistic targets have CSAS signatures with trivial **QuasiP**( $u$ ), limiting its usefulness. Although **Const**( $u$ ) does not share this second limitation, we have not succeeded in discovering an algorithmically computable characterisation of it.

This article establishes the following new results:

- (1) The factorisation categories are functorial (Propositions 8, 9, and 16), changing the domain or codomain induces functors on the factorisation categories;
- (2) The factorisation categories are related to, but distinct from, homotopy classes (Corollary 3 and Proposition 14);
- (3) When maps are related via a diffeomorphism, their respective categories are isomorphic (Theorem 1) and the image of **CRSE** in them is maximal (Theorem 4);
- (4) When the same target appears in multiple settings, the factorisation categories of the resulting signatures have equivalent subcategories based on the target (Theorems 3 and 5); and
- (5) When the domain  $M$  is a circle  $S^1$  (directly relevant to CSAS), the quasiperiodic factorisation category is completely classified by subgroups of the fundamental group of  $N$  (Theorem 2).

## 2. Motivating example: CSAS

Consider a CSAS collection in which the sonar platform orbits a fixed target, as shown in Figure 1. For the purposes of this article, suppose that the sensor's *standoff range*  $R$  is constant, and that its *look angle*  $\theta$  increases monotonically (but not necessarily linearly) from  $0^\circ$  to  $360^\circ$  over the length of the collection. If the target's scatterers are sufficiently reflective when compared to the receiver noise and clutter in the scene, then determining the ranges to them is not a difficult problem. This fact means that we may safely

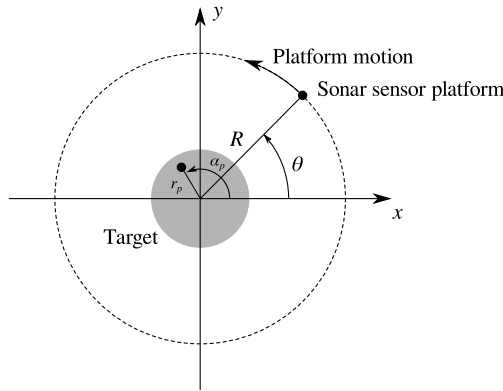


**Figure 1.** General CSAS collection geometry wherein the sensor platform orbits a target, where one scatterer’s position has been highlighted.

assume that the standoff range  $R$  is fixed and constant without impacting the realism of the model. If the actual range varies, this may be compensated for by applying a  $\theta$ -dependent modulation to the raw echoes.

We will follow mathematical tradition and denote the set of angles by the circle  $S^1$  so that  $\theta \in S^1$  specifies the look angle. The sensor emits *sonar pulses* as it moves along its trajectory and records their echoes from the target. We will neglect receive and transmit filter effects for this article to keep the exposition simple, though filters can be incorporated easily using the framework the article develops. Let us therefore assume that the transmitted pulses are impulses, and the sensor’s receiver covers a wide band of frequencies.

Given the standoff range  $R$  and a point scatterer located at a distance  $r_p$  to target centre, with an angle  $\alpha_p$  relative to the the  $\theta = 0$  axis, the quantity  $r_p \cos(\alpha_p - \theta)$  is the component of the vector from the scatterer to the sensor along the look direction. (See Figure 1.) Likewise,  $r_p \sin(\alpha_p - \theta)$  is the component of the vector from the scatterer to the sensor that is normal to the look direction. Therefore, the distance from the scatterer to the sensor is

$$x = \sqrt{(r_p \sin(\alpha_p - \theta))^2 + (R + r_p \cos(\alpha_p - \theta))^2},$$

If the signal wavelength is  $2\pi f/c$ , where  $f$  is the frequency of the sonar pulse and  $c$  is its phase speed, then the amount of phase delay along a path of length  $x$  is  $2\pi fx/c$ . This is generally expressed as a complex factor  $\exp(-2\pi ifx/c)$ . If the standoff range  $R$  is large, we can approximate the phase delay from the scatterer to the sensor via

$$\begin{aligned} \exp(-2\pi ifx/c) &= \exp\left(-\frac{2\pi if}{c} \sqrt{(r_p \sin(\alpha_p - \theta))^2 + (R + r_p \cos(\alpha_p - \theta))^2}\right) \\ &\approx \exp\left(-\frac{2\pi if}{c} r_p \cos(\alpha_p - \theta)\right) \exp\left(-\frac{2\pi if}{c} R\right). \end{aligned}$$

The nuisance phase  $\exp(-\frac{2\pi if}{c} R)$  is traditionally absorbed into a multiplicative factor dependent on the scatterer’s material properties called its *complex reflectivity*  $a_p$ .

Assembling these pieces, the following equation models the *signature*  $s$ , which describes the received echoes as a function of the look angle  $\theta$  and received frequency  $f$  received from a set of  $P$  point scatterers,

$$s(\theta, f) = \sum_{p=1}^P \frac{a_p \exp\left(-\frac{2\pi if}{c} r_p \cos(\alpha_p - \theta)\right)}{\sqrt{(r_p \sin(\alpha_p - \theta))^2 + (R + r_p \cos(\alpha_p - \theta))^2}}. \tag{2.1}$$

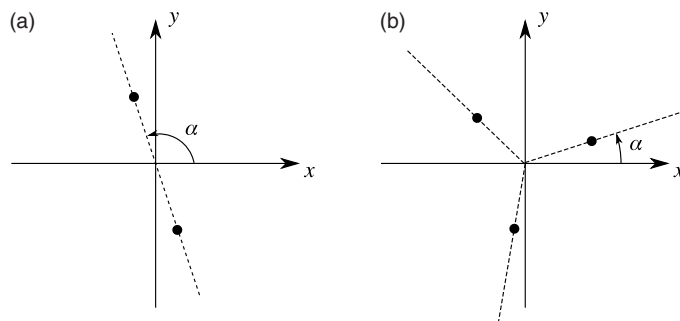


**Figure 2.** Two simple composite scatterers (a) one with 2-fold symmetry and (b) one with 3-fold symmetry.

The denominator in each term captures the fact that the echo from a given scatterer spreads out, making its received signal strength diminish as its distance to the sensor increases.

This is, of course, a rather simplified model. Substantially more realistic models (not just superpositions of point scatterers) are supported by the framework developed in the latter sections of this article. Although we use a single look angle  $\theta$  in this section, this is only to ensure that the signals can be represented ‘on paper’ as images. The framework supports ‘look angles’ that can be represented as points on an arbitrary connected smooth manifold.

Equation (2.1) sets up a correspondence between the look angle  $\theta$  and the received echo as a function of pulse frequency  $f$ . If the sensor platform’s angular position with respect to the target is not known accurately, this function becomes the composition of  $s$  with an unknown function of *slow time*  $t$ . That is,  $\theta = \phi(t)$ , where  $t$  is the time of pulse transmission. Due to the inertia of the sensor platform, we may assume that the function  $\phi$  is smooth.

If  $\phi$  is an affine function, then traditional imaging methods (for instance, polar format or back projection [41]) provide a complete solution to the problem of determining the location and reflectivity of each scatterer. These methods do not work at all if  $\phi$  is an unknown smooth function that deviates far from an affine function.

To fix ideas, let us restrict attention to the case where the point scatterers in this target model can be grouped into two subsets: one subset has a  $180^\circ$  rotational symmetry, while the other subset has a  $120^\circ$  rotational symmetry. We will usually refer to these symmetries as a *2-fold symmetry* and a *3-fold symmetry*, respectively. One easy way that this may happen is if the first subset consists of exactly two point scatterers, placed opposite the target centre, as in Figure 2(a). Similarly, the other subset could be realised as a subset of exactly three point scatterers, evenly spaced around a circle concentric with the target centre, as in Figure 2(b). It is immediately clear that there are other possible ways to realise these kinds of symmetries using more point scatterers, and while this will be developed more completely in Proposition 5 (and following), these two simplistic models will suffice for the moment. We will call these subsets of the set of point scatterers *composite scatterers* for brevity. Notice that each composite scatterer additionally has a *reference rotation angle*  $\alpha$  with respect to the  $\theta = 0$  axis. The two composite scatterers will typically have different reference rotation angles, which means that the superposition of the two composite scatterers may not have any rotational symmetries at all.

### 2.1. A composite scatterer model: Quasiperiodic factorisations

The general formula (2.1) can be specialised to two subsets of scatterers, one with  $P$ -fold symmetry and one with  $Q$ -fold symmetry. If we assume that the composite scatterer with  $P$ -fold symmetry consists of

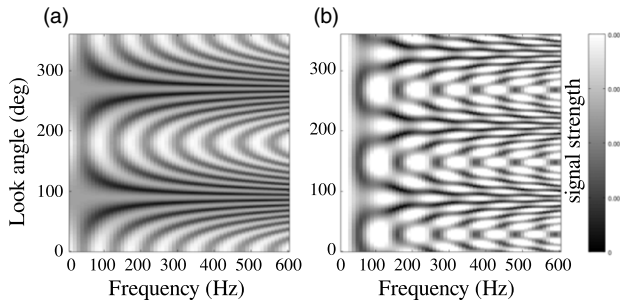


**Figure 3.** Signatures of the composite scatterers shown in Figure 2 (a) has 2-fold symmetry and (b) has 3-fold symmetry.

exactly  $P$  points, then the signature reduces to a rather specific form:

$$s_P(\theta, f; \alpha) = a \sum_{p=1}^P \frac{\exp\left(-\frac{2\pi if}{c} r \cos\left(\frac{2\pi p}{P} + \alpha - \theta\right)\right)}{\sqrt{\left(r \sin\left(\frac{2\pi p}{P} + \alpha - \theta\right)\right)^2 + \left(R + r \cos\left(\frac{2\pi p}{P} + \alpha - \theta\right)\right)^2}}, \tag{2.2}$$

in which all of the point scatterers have the same complex reflectivity  $a = a_p$  and the same distance to target center  $r = r_p$ . Because  $\cos$  and  $\sin$  are  $2\pi$ -periodic functions, and the sum consists of  $P$  evenly spaced terms, it follows that  $s(\theta + (2\pi/P), f) = s(\theta, f)$  for all look angles  $\theta$  and frequencies  $f$ .

Example signatures of the two scatterers shown in Figure 2 are shown in Figure 3. In the plots of the signatures, the look angle  $\theta$  is shown in the vertical dimension and the frequency  $f$  is shown on the horizontal dimension. Notice that both of the signatures repeat vertically, with the 2-fold symmetric target showing two copies and the 3-fold symmetric target showing three copies. It is therefore obvious that the symmetry class can be used to coarsely discriminate between targets, as the two signatures shown in Figure 3 are easy to distinguish from each other.

Concretely, the signatures corresponding to two targets with 3-fold symmetry will repeat three times in look angle, like Figure 3(b). The structure of the signature within one period of this repetition – within a horizontal band  $120^\circ$  tall in Figure 3(b) – can be used to distinguish two different targets with 3-fold symmetry. Generalising this idea, two targets with the same symmetry class can be discriminated by comparing their fundamental domains.

If the trajectory of the sensor is unevenly traversed so that the look angle does not vary linearly, then the periodicity visible in Figure 3 is destroyed. In this case, sonar engineers often call the distorted angular coordinate *slow time*, since it measures the time as the sensor moves along its trajectory. (In like manner, *fast time* is often used for the time within a pulse, which is a distorted version of the distance from the sensor to the target.) For instance, Figure 4 shows two possible signatures after a smooth trajectory distortion has been applied, though only one complete orbit around the target has been traversed. To relate the vertical axes in the plots shown in Figure 4 to those of Figure 3, one must transform slow time  $t$  to look angle  $\theta$  by integrating the sensor’s angular velocity:

$$\theta = \phi(t) = \int_0^t \phi'(t) dt.$$

In order to do this, one must have a good measurement of the angular velocity. In practice, this is often difficult.

Although Figures 3(b) and 4(a) are collections of echoes from the same composite scatterer and differ only by the application of a distortion  $\phi$ , they are quite different as functions. On the other hand, no trajectory distortion of Figure 4(b) can be applied to transform it into any of the others because its underlying symmetry class (5-fold symmetry) is different.

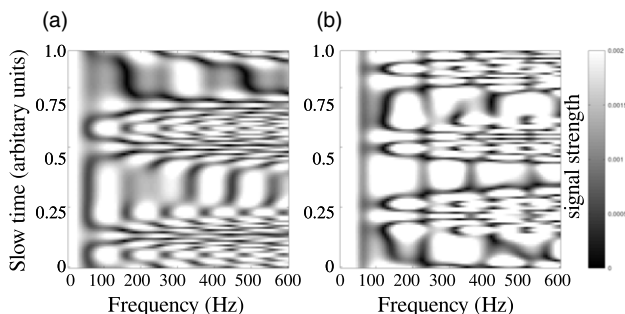


**Figure 4.** Signatures of the composite scatterers with trajectory distortions over a single orbit of the target; after removing distortions (a) has 3-fold symmetry and (b) has 5-fold symmetry.

This article aims to make the intuitive ideas of ‘removing trajectory distortions’ precise, and develops the proper notion of ‘signatures equivalent up to trajectory distortions’. The main idea is to realise that the signatures shown in Figure 3 can act as representatives of signature equivalence classes and to consider the properties arising from trajectory distortions. Mathematically, decoupling trajectory effects from target effects requires that we consider the process of *factoring functions via composition*.

As a preview, Theorem 2 characterises factorisations of functions with circular domains. Intuitively, it says that one may distinguish the equivalence classes of signatures by their winding numbers. In other words, even though the rows of Figure 4(a) do not traverse look angles evenly, they repeat three times. This differs from Figure 4(b), which makes five repetitions, and so the signatures must be different. On the other hand, the signature in Figure 3(b) also makes three repetitions, so there are grounds for possible equivalence with Figure 4(a). Moreover, if we are considering only one frequency (column in Figures 3 and 4), then Corollary 2 indicates that this is *all* that can be determined. We emphasise that none of these conclusions are surprising in the case that the trajectory is evenly traversed – the trajectory has been motion compensated to look angle – but we reiterate that ensuring trajectories are evenly traversed can be quite difficult in practice.

## 2.2. Two composite scatterers: Constant rank factorisations

For a target formed as the superposition of two composite scatterers, Proposition 5 shows that the signature traces out a *torus knot*, a closed path on the surface of a torus. This remains true if there are trajectory distortions. As a result, Theorem 2 states that such signatures can be classified by the topological type of the corresponding torus knot. Torus knots are classified by a pair of integer winding numbers  $(P, Q)$ , which correspond to the symmetry classes of the composite scatterers.

Again using the look angle  $\theta$  directly to fix ideas, we can construct the superposition of both subsets of scatterers, a  $P$ -fold symmetric subset and a  $Q$ -fold symmetric subset. This is done by taking a sum<sup>1</sup> of the two composite scatterers:

$$s(\theta, f; \alpha, \alpha') = s_P(\theta, f; \alpha) + s_Q(\theta, f; \alpha'). \quad (2.3)$$

It is sometimes helpful to consider the *relative angle*  $\beta = \alpha' - \alpha$ . Figure 5 shows the configuration of point scatterers if  $P = 2$ ,  $Q = 3$ , and  $\beta = 28^\circ$ .

<sup>1</sup>It will become apparent that equation (2.3) satisfies the hypotheses of Proposition 5. Given this fact,  $s$  has a *constant rank factorisation* in which the *phase function* is a torus knot.



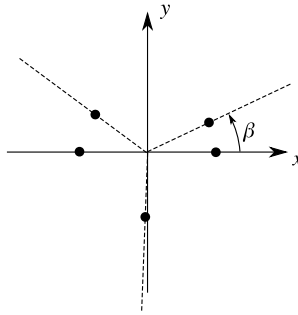


Figure 5. Combined scatterer with  $P = 2$ ,  $Q = 3$ , and relative angle  $\beta = 28^\circ$  shown.

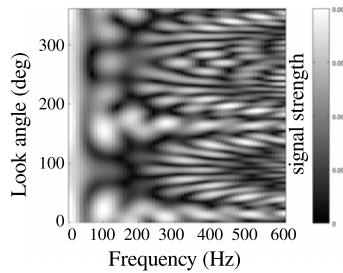


Figure 6. A typical signature of the sum of the two scatters shown in Figure 5, where  $P = 2$ ,  $Q = 3$ , and the relative angle is  $\beta = 28^\circ$ .

Since the  $\theta = 0$  axis was essentially arbitrary, it is sometimes helpful to take  $\alpha = 0$ , resulting in the formula:

$$s(\theta, f; 0, \beta) = a \sum_{p=1}^P \frac{\exp\left(-\frac{2\pi if}{c} r \cos\left(\frac{2\pi p}{P} - \theta\right)\right)}{\sqrt{\left(r \sin\left(\frac{2\pi p}{P} - \theta\right)\right)^2 + \left(R + r \cos\left(\frac{2\pi p}{P} - \theta\right)\right)^2}} + a' \sum_{q=1}^Q \frac{\exp\left(-\frac{2\pi if}{c} r' \cos\left(\frac{2\pi q}{Q} + \beta - \theta\right)\right)}{\sqrt{\left(r' \sin\left(\frac{2\pi q}{Q} + \beta - \theta\right)\right)^2 + \left(R + r' \cos\left(\frac{2\pi q}{Q} + \beta - \theta\right)\right)^2}}$$

For simplicity, let us take  $a = a'$  and  $r = r'$  in what follows in this section. The resulting signature is shown in Figure 6.

Notice that superposition of these particular two subsets (Figure 5) is not quite 2-fold symmetric itself, because  $28^\circ + 240^\circ = 268^\circ \neq 270^\circ$ . It would be 2-fold symmetric if the relative angle were to be chosen as  $\beta = 30^\circ$ , and there are other possible choices of relative angle resulting in a 2-fold symmetric target. The effect of this slight asymmetry is visible in Figure 6, where it makes the signature approximately repeat vertically.

After inspecting equation (2.2), it is clear that holding  $\theta$  fixed and varying  $\alpha$  results in the same information as varying  $\theta$  while holding  $\alpha$  fixed. With two reference angles in equation (2.3), it is more convenient to hold the look angle  $\theta$  fixed and vary the reference angles instead. If we hold the look angle  $\theta$  and frequency  $f$  fixed, while varying the reference angles  $\alpha$  and  $\alpha'$  arbitrarily, we obtain a somewhat different perspective of the signature, shown for two different frequencies in Figure 7.

The benefit of this perspective is that all possible relative angles  $\beta$  are represented. The locus of points in Figure 7 with a fixed relative angle  $\beta = \alpha' - \alpha$  is a line with slope of 1. The relative angle  $\beta$

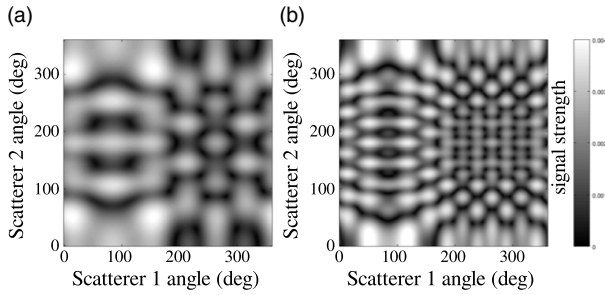


Figure 7. Response as a function of scatterer angles at (a) 300 Hz and (b) 600 Hz.

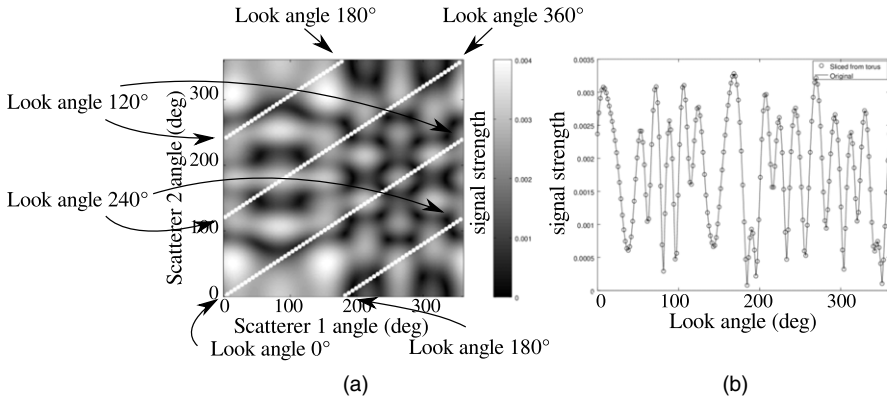


Figure 8. Extracted single-frequency response with a constant relative angle ( $28^\circ$ ) between scatterers at 300 Hz.

determines the intercept of the line. For instance, if  $\beta = 28^\circ$ , Figure 8 shows how the signature at 300 Hz is obtained by following such a trajectory.

The plots shown in Figures 7(a)–(b) and 8(a) are really on the surface of a torus in virtue of Proposition 5, since both the horizontal and vertical axes measure angles. The trajectory shown in Figure 8(a) for a relative angle  $\beta = 28^\circ$  eventually returns to its starting point (at the origin), after making two complete horizontal circuits and three complete vertical circuits in Figure 8(a). The trajectory is therefore an example of a (2, 3) torus knot, as is immediately apparent when drawn on the surface of an embedded torus in Figure 9(a). The signature is therefore best thought of as a function on the surface of the torus, since it too is periodic in both reference angles. If we consider a different frequency, say 600 Hz, then the torus knot trajectory is unchanged, but the underlying function on the surface of the torus changes, as shown in Figure 9(b). Considering *all* frequencies  $f$  is theoretically (and practically) valuable but is difficult to draw.

The functions on the surface of the torus in Figure 9 allow us to go beyond merely classifying signatures by torus knot type. If two targets have the same torus knot type, they can still be distinguished by differences between their corresponding functions on the torus. If we switch to a different target, the torus functions will change, probably substantially, and will no longer assure the same kind of equivalence. Therefore, the basic idea given two signatures is to first determine if they have the same torus knot type. If not, they correspond to different targets. If they do have the same torus knot type, then one would hope to simulate the functions on the torus and argue based on their specifics.

The mathematical invariants explored in this article characterise (theoretically) how close the two signatures are by parameterising *all* possible functions on the torus, and on all other manifolds besides.

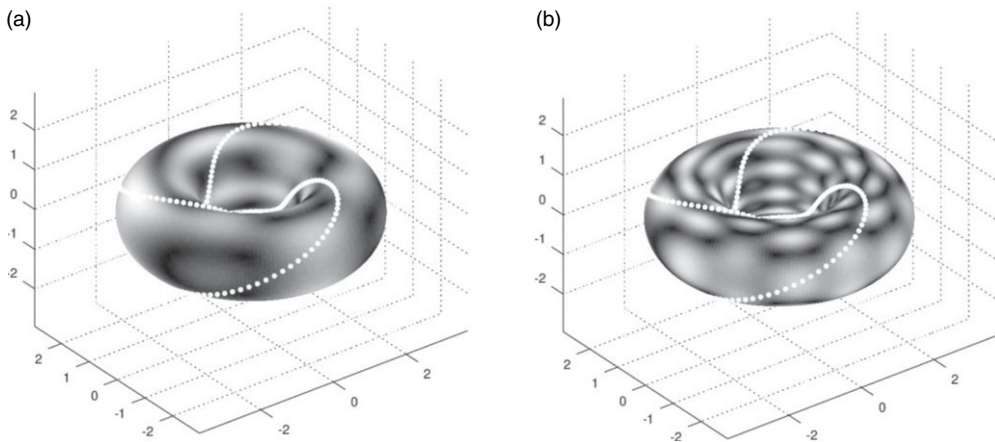


**Figure 9.** Single-frequency response with a constant relative angle ( $28^\circ$ ) as a torus knot at (a) 300 Hz, (b) 600 Hz.

While these invariants are *emphatically not yet practically computable*, their use provides a theoretical framework for asserting that two targets are distinguishable *regardless* of trajectory distortions.

The key insight is that distorting the sensor trajectory deflects the knot on the surface of the torus but cannot change its torus knot type. Effectively, because the knot is constrained to lie on the surface of the torus, its knot type is ‘locked in place’. This article defines *constant rank factorisations* to model trajectory distortions in this case. Moreover, the article defines an equivalence class that classifies these factorisations. The article presents several tools to characterise the mathematical properties of constant rank factorisations (Theorems 3 and 5) and presents a complete characterisation (Theorem 2) that applies to  $P$ -fold symmetric targets.

### 3. Categories of factorisations

We begin by generalising the ideas inherent in Section 2. Given the nature of the sensing problem, the collected data are measured in a *signal space*  $N$ , which is typically a submanifold of  $\mathbb{C}^n$ . For instance, the signal space is  $\mathbb{C}^n$  in equations (2.1) (2.2), and (2.3) if  $n$  distinct frequencies are collected from each sensor location along the trajectory.

Similarly, the sensor’s configuration (location, time, etc.) is captured by a manifold  $M$ . We assume that a signature of our target is characterised by an idealised representative target model represented as a smooth map between two spaces  $U : C \rightarrow N$ , and that the sensor trajectory can be modelled by composing this idealised model with a function  $\phi : M \rightarrow C$ , which may contain distortions. We cannot measure either of these functions, but instead are able to measure their composition  $u = U \circ \phi$ . In order to make any theoretical headway, some assumptions must be placed on the functions  $\phi$  or  $U$ . This article relies on the idea that the trajectory does not ‘come to a stop’ at any point. This can be modelled formally by requiring the Jacobian matrix  $d\phi$  to have a constant rank throughout  $M$ .

**Definition 1.** A smooth map  $f : M \rightarrow N$  is said to be of constant rank if the Jacobian matrix  $d_f$  has the same rank at every point  $x$  in  $M$ . For brevity, the rank of the Jacobian matrix for a constant rank map will be called the rank of  $f$ .

Constant rank maps have many useful properties that avoid some pathological behaviours of continuous maps. Most importantly, a constant rank map imposes restrictions on the dimension of its domain and image.

**Proposition 1.** [31, Thm. 7.15] *Suppose that  $f : M \rightarrow N$  is a smooth map with constant rank:*

- (1) *If  $f$  is surjective, then it is a submersion: its rank is equal to the dimension of  $N$ ,*
- (2) *If  $f$  is injective, then it is an immersion: its rank is equal to the dimension of  $M$ , and*
- (3) *If  $f$  is bijective, then it is a smooth embedding: its rank is equal to the dimension of  $M$ , and this is the same as the dimension of  $N$ .*

When these special cases are not available, the constant rank assumption still provides bounds on the dimensions involved.

**Proposition 2.** *Suppose that  $f : M \rightarrow N$  is a smooth map from an  $m$ -dimensional manifold to an  $n$ -dimensional manifold, and that  $f$  has constant rank  $k$ . Then  $k \leq m$ , and the image of  $f$  is a  $k$ -dimensional immersed submanifold of  $N$ .*

*Proof.* Briefly, this follows by applying [31, Thm 7.13] and [31, Lem. 8.18]. The former asserts that there are coordinate charts on  $M$  and  $N$  where  $f$  can be written as:

$$f(x_1, \dots, x_k, x_{k+1}, \dots, x_m) = (x_1, \dots, x_k, 0, \dots, 0).$$

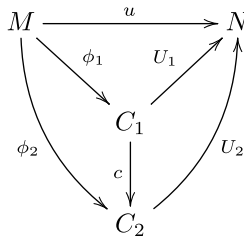
Observe that  $k \leq m$  is a consequence of this fact. One then notes that the chart in question on  $N$  is a submanifold chart for (a portion of) the image of  $f$ . Restricting the domain to the  $k$ -dimensional submanifold  $S \subseteq M$  whose coordinate charts select the first  $k$  coordinates in the formula above, the result is clearly an immersion since  $f|_S$  is injective on each of the relevant charts. At this point, [31, Lem. 8.18] asserts that  $f|_S$  is locally an embedding, resulting in the dimension  $k$  for the image.  $\square$

**Corollary 1.** *A constant rank map cannot be a surjection from a lower-dimensional manifold to a higher-dimensional manifold.*

In particular, if the domain is  $S^1$  as is the case for CSAS, the rank of the Jacobian cannot exceed 1.

**Definition 2.** *A constant rank factorisation of a smooth map  $u : M \rightarrow N$  between two finite-dimensional smooth manifolds is a factorisation  $u = U \circ \phi$  in which  $\phi$  is a smooth map of constant rank. If we write  $\phi : M \rightarrow C$  and  $U : C \rightarrow N$  for a constant rank factorisation, we call  $C$  the phase space,  $\phi$  the phase map, and  $U$  the signature map. We will often write a constant rank factorisation  $u = U \circ \phi$  as an ordered pair  $(\phi, U)$  when the function  $u$  is understood from context. We will permit the phase space  $C$  to be a smooth metrizable manifold modelled on separable Hilbert space of any dimension,<sup>2</sup> including infinity.*

A morphism  $C : (\phi_1, U_1) \rightarrow (\phi_2, U_2)$  between two constant rank factorisations of a single map  $u : M \rightarrow N$  consists of a commuting diagram<sup>3</sup>



where  $c : C_1 \rightarrow C_2$  is a smooth map, which we call the component map. Because the diagram commutes, this means that  $\phi_2 = c \circ \phi_1$  and  $U_1 = U_2 \circ c$ .

<sup>2</sup>If  $C$  is a finite-dimensional smooth manifold, it is automatically metrizable [31, Prop. 11.26] and modeled on separable Hilbert space.

<sup>3</sup>A diagram is said to *commute* if the functions obtained by composing adjacent arrows depend only on their start and end points in the diagram. Commutative diagrams are an efficient way to express a collection of functional equations and make frequent appearances in this article.

In the CSAS example in Section 2, the path of the sensor defines the manifold  $M = \mathbb{R}$ . The signal space is  $N = \mathbb{C}^n$  where  $n$  is the number of frequency samples collected. Finally, the phase space  $C = S^1$  is the look angle. As a result, Figures 3 and 6 show examples of three signature maps ( $U$  functions). In contrast, Figure 4 shows two examples of  $u = U \circ \phi$  functions.

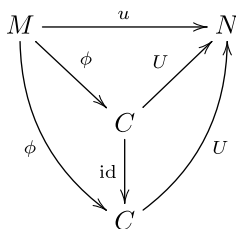
Objects and morphisms form the building blocks of a category.

**Definition 3.** [51, Def. 5.1.1.1][24, Sec. 2.3] A category  $\mathbf{C}$  consists of a collection of objects and morphisms. Each morphism  $m$  is associated with an ordered pair of objects  $(x,y)$ , which is usually written  $m : x \rightarrow y$ . If  $m_1 : x \rightarrow y$  and  $m_2 : y \rightarrow z$  are two morphisms, there is a unique morphism called the composition  $(m_2 \circ m_1) : x \rightarrow z$ . Composition is an associative operation so that  $(m_1 \circ m_2) \circ m_3 = m_1 \circ (m_2 \circ m_3)$ . Moreover, for every object  $x$ , there is a unique morphism  $id_x : x \rightarrow x$  for which  $id_x \circ m = m$  and  $n \circ id_x = n$  for any morphisms  $m : y \rightarrow x$  and  $n : x \rightarrow z$ .

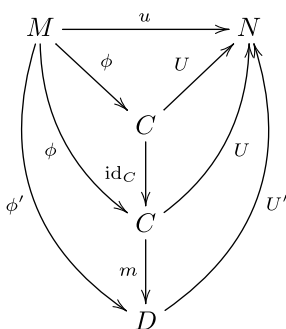
**Lemma 1.** The class of constant rank factorisations of a smooth map  $u : M \rightarrow N$  forms a category  $\mathbf{Const}(u)$ , where the composition of morphisms of constant rank factorisations consists of composition of component maps between the phase spaces.

*Proof.* We take each constant rank factorisation  $u = U \circ \phi$  as an object in  $\mathbf{Const}(u)$ .

Using the identity function for the component map, the morphism  $id_{(\phi,U)} : (\phi, U) \rightarrow (\phi, U)$  given by the diagram



does not change any other morphism when it is composed on the left or the right. For instance, abusing notation slightly, if  $m : (\phi, U) \rightarrow (\phi', U')$  is another morphism whose component map is  $m$ , then we have the larger diagram



that defines the composition  $m \circ id_{(\phi,U)}$ . Evidently the component map of this composition is  $m = m \circ id_C$ , which asserts that on the level of  $\mathbf{Const}(u)$  morphisms, we have that  $m = m \circ id_{(\phi,U)}$ . Composition on the left by  $id_{(\phi,U)}$  follows similarly.

Suppose that we have three morphisms  $m_1 : (\phi_1, U_1) \rightarrow (\phi_2, U_2)$ ,  $m_2 : (\phi_2, U_2) \rightarrow (\phi_3, U_3)$ , and  $m_3 : (\phi_3, U_3) \rightarrow (\phi_4, U_4)$ . Associativity of composition of these morphisms  $(m_1 \circ m_2) \circ m_3 = m_1 \circ (m_2 \circ m_3)$  follows because the same equation holds for their corresponding component maps.  $\square$

One general source of constant rank factorisations is *quasiperiodic factorisations*, which were defined in several earlier papers.

**Definition 4.** [47, 48] A quasiperiodic factorisation of a smooth map  $u : M \rightarrow N$  consists of a factorisation  $u = U \circ \phi$  in which  $\phi$  is a smooth submersion. The category of quasiperiodic factorisations  $\mathbf{QuasiP}(u)$  is defined analogously to  $\mathbf{Const}(u)$ , with objects consisting of factorisations and morphisms given by diagrams of exactly the same form as in Definition 2.

**Proposition 3.** Every quasiperiodic factorisation is also a constant rank factorisation. Thus, the category of quasiperiodic factorisations  $\mathbf{QuasiP}(u)$  is a subcategory of the category of constant rank factorisations  $\mathbf{Const}(u)$ .

*Proof.* Observe that a submersion is necessarily of constant rank. □

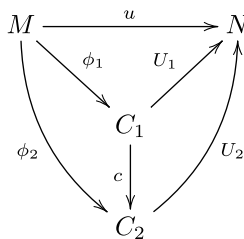
The trivial factorisation of a smooth map  $u = u \circ \text{id}$  arises when the trajectory is *not* distorted, since the phase map is simply the identity map. Such a situation is an instance of a general phenomenon, called an *initial object*.

**Definition 5.** [51, Def. 6.1.3.2][24, Sec. 3.5] An object  $i$  in a category is called *initial* if for every object  $x$  there is exactly one morphism  $i \rightarrow x$ .

Both categories  $\mathbf{QuasiP}(u)$  and  $\mathbf{Const}(u)$  share an initial object.

**Proposition 4.** The factorisation of a smooth map  $u : M \rightarrow N$  given by  $u = u \circ \text{id}_M$  is an initial object for  $\mathbf{Const}(u)$  and an initial object for  $\mathbf{QuasiP}(u)$ .

*Proof.* To establish this, suppose that  $u = U \circ \phi$  is another constant rank (or quasiperiodic) factorisation. The only way to make the following diagram commute



for some manifold  $C$  is to assert that  $c = \phi$ . Conversely, with  $c = \phi$ , this diagram always commutes! □

Section 2 provides anecdotal evidence that certain sonar collections can be described by torus knots. This is a general situation that arises whenever two periodic smooth functions are superposed.

A *torus knot* is a smooth embedding  $\phi : S^1 \rightarrow S^1 \times S^1$ . That means that  $\phi$  has a Jacobian map of rank 1 at all points in  $S^1$  and is a homeomorphism onto its image [31, Ch. 7]. As a result, a torus knot cannot have self-intersections. This definition is somewhat more specific than the usual definition of a knot in the literature, which merely requires continuity. Equivalence classes of torus knots are characterised by a pair of coprime integers, called the *torus knot type* [35].

**Proposition 5.** If  $u : S^1 \rightarrow \mathbb{C}^D$  is the sum

$$u(x) = u_1(x) + u_2(x)$$

of two non-constant smooth functions, a  $(2\pi/m)$ -periodic function  $u_1$ , and a  $(2\pi/n)$ -periodic function  $u_2$  for integers  $m$  and  $n$ , then  $u$  has a constant rank factorisation in which the phase function is a torus knot of type  $(m,n)$ .

Notice in particular that a torus  $S^1 \times S^1$  is of larger dimension (the dimension is 2) than that of the circle  $S^1$ . Therefore, the constant rank factorisation guaranteed by this Proposition is *not* a quasiperiodic factorisation. On the other hand, projecting to either of the two factors  $S^1 \times S^1 \rightarrow S^1$  yields a quasiperiodic factorisation.

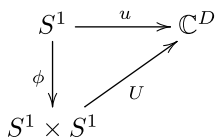
*Proof.* Let  $\phi_1, \phi_2 : S^1 \rightarrow S^1$  be linear maps of degree  $m$  and  $n$ , respectively, so that

$$\phi_1(x) := [mx]_{2\pi}, \text{ and } \phi_2(x) := [nx]_{2\pi}.$$

According to [47, Thm. 8], this choice results in the *universal quasiperiodic factorisations*<sup>4</sup> of  $u_1$  and  $u_2$  provided  $m$  and  $n$  are coprime. If we define  $\phi : S^1 \rightarrow (S^1 \times S^1)$  by:

$$\phi(x) := (\phi_1(x), \phi_2(x)) = ([mx]_{2\pi}, [nx]_{2\pi})$$

then, by hypothesis



commutes if we take

$$U(y, z) := u_1(y) + u_2(z).$$

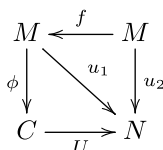
By construction,  $\phi$  is of constant rank and is also a torus knot of type  $(m, n)$ . □

The categories **Const**( $u$ ) and **QuasiP**( $u$ ) are diffeomorphism invariants.

**Theorem 1.** *Suppose that  $u_1, u_2 : M \rightarrow N$  are smooth maps and  $M$  is a connected manifold. If  $u_2 = u_1 \circ f$  where  $f : M \rightarrow M$  is a diffeomorphism, then*

- (1) **Const**( $u_1$ ) and **Const**( $u_2$ ) are isomorphic categories, and
- (2) **QuasiP**( $u_1$ ) and **QuasiP**( $u_2$ ) are isomorphic categories.

*Proof.* Both statements follow from reasoning about the following commutative diagram



for an arbitrary constant rank (or quasiperiodic factorisation)  $u_1 = U \circ \phi$ . Evidently this implies that  $u_2 = U \circ \phi \circ f$  is a factorisation of the same type, since diffeomorphisms are of locally constant rank and we assumed that  $M$  is connected. This provides for a bijection on the objects of the two categories under discussion. Since this also means that the factorisations of  $u_1$  and  $u_2$  share the space  $C$ , there is no further transformation required on morphisms to establish the isomorphism. □

A given smooth map  $u$  often has many quasiperiodic factorisations, though there is a ‘simplest’. This notion can be formalised by the dual notion of an initial object, namely a *final object*. A final object  $f$  in a category is one for which every other object  $x$  has a unique morphism  $x \rightarrow f$ . In **Const**( $u$ ), morphisms may only be unique up to composition with a diffeomorphism.

The ‘simplest’ quasiperiodic factorisation is the one given by the final object of **QuasiP**( $u$ ). That these final objects always exist is suggested by the construction in [47, Thm. 5].

**Proposition 6.** *The category of quasiperiodic factorisations **QuasiP**( $u$ ) of a smooth map  $u : M \rightarrow N$  has final objects.*

In [47], these are called *universal quasiperiodic factorisations*.

*Proof.* The construction in [47, Thm. 5] produces a factorisation  $u = U \circ \phi$  with phase space  $C$  in which  $C$  is a particular quotient of the disjoint union of all phase spaces for quasiperiodic factorisations. That is,

<sup>4</sup>As will be discussed in Proposition 6, these are also *final objects* in **QuasiP**( $u_1$ ) and **QuasiP**( $u_2$ ).

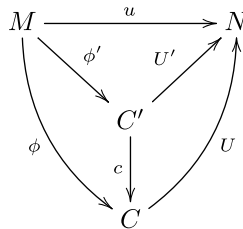
$$C = \left( \bigsqcup_{\alpha} C_{\alpha} \right) / \sim,$$

where  $\alpha$  ranges over all quasiperiodic factorisations. The equivalence relation  $\sim$  is defined by  $x_1 \sim x_2$  whenever  $x_1 \in C_1$  and  $x_2 \in C_2$  are points in the phase spaces for two quasiperiodic factorisations  $u = U_1 \circ \phi_1 = U_2 \circ \phi_2$ , and there is an  $x$  such that  $x_1 = \phi_1(x)$  and  $x_2 = \phi_2(x)$ . Such a  $C$  is clearly well defined as a set. To establish that  $C$  is a manifold as well, it suffices to realise that every value in the codomain of a surjective submersion is a regular value. The preimage of every value is therefore a submanifold of the domain. Continuity of the phase maps ensures that preimages of open sets around each value in the codomain are open as well, so the equivalence relation  $\sim$  identifies open sets to each other, preserving coordinate charts. As a result,  $C$  is a manifold of dimension

$$k = \min\{\text{rank } \phi : u = U \circ \phi \text{ is a quasiperiodic factorisation}\}.$$

This, being a minimum of a set of non-negative integers, not only exists but is attained. (The dimension is important to keep in mind for **Const**( $u$ ) in Proposition 7.)

It remains to establish that if  $u = U' \circ \phi'$  is another quasiperiodic factorisation with phase space  $C'$ , then there is a unique morphism  $c : C' \rightarrow C$  making the diagram below commute,



Since  $C'$  is one of the sets appearing in the disjoint union, there is a smooth map  $c : C' \hookrightarrow \bigsqcup C_{\alpha} \rightarrow C$  formed as the composition of two constant rank maps.

Suppose that there were another choice  $c' : C' \rightarrow C$  making the diagram commute. Consider  $x \in C'$ . Since  $\phi'$  is surjective by assumption, there is a  $y \in M$  such that  $\phi'(y) = x$ . Since the diagram commutes, this means that  $\phi(y) = c'(\phi'(y)) = c'(x)$ . Moreover, commutativity for the other morphism implies that  $\phi(y) = c(\phi'(y)) = c(x)$ . Therefore, we must conclude that  $c'(x) = c(x)$ , establishing uniqueness of  $c$ .  $\square$

Although final objects in **Const**( $u$ ) must necessarily involve infinite-dimensional phase spaces, they are actually a bit easier than you might imagine because infinite-dimensional manifolds have simpler structure than finite-dimensional ones.

**Proposition 7.** *The final object of **Const**( $u$ ) for every smooth map  $u : M \rightarrow N$  between finite-dimensional manifolds has the same phase space, namely infinite-dimensional separable Hilbert space. Moreover, the final object's phase map is an embedding of the phase space of the final object of **QuasiP**( $u$ ) as a finite-dimensional submanifold into this common phase space.*

*Proof.* Note that the phase map in question is definitely of finite rank – being the same rank as in **QuasiP**( $u$ ) because every quasiperiodic factorisation is also a constant rank factorisation. To see that the phase space is correct, suppose that we have any other **Const**( $u$ ) object, a constant rank factorisation  $u = U' \circ \phi'$  with phase space  $C'$ . Restricting the codomain to the image of the phase map  $\phi'(M)$ , we are back at a **QuasiP**( $u$ ) factorisation, so we obtain a uniquely determined map into the claimed phase space on that portion via Proposition 6.

If the factorisation's phase space  $C'$  is finite-dimensional, there is no further work to do as the portion outside the image of  $\phi'$  is finite-dimensional and can be easily embedded in infinite-dimensional Hilbert space. Otherwise, as a consequence of Henderson's theorem [29, Cor. 1], the factorisation's phase space  $C'$ , being a metrizable infinite-dimensional manifold modeled on separable Hilbert space, embeds as an



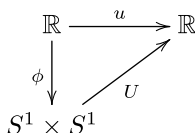
open set in separable infinite-dimensional Hilbert space itself. This establishes the required map into the final object’s phase space. Because the morphism is an embedding, we have the usual fact that two embedded copies of the same manifold are diffeomorphic to each other. Therefore, the map is unique up to a diffeomorphism. □

At this point, it likely seems that constant rank factorisations and quasiperiodic factorisations are rather similar. The key difference between these two concepts is crystallised by the idea of an embedded torus knot  $u : S^1 \rightarrow (S^1)^n \subset \mathbb{R}^{n+1}$ . Every quasiperiodic factorisation of  $u$  will necessarily have a one-dimensional phase space due to the requirement that the phase map be a surjective submersion. (Moreover, see Lemma 2 proven a little later in this article.) In contrast, factorisation of  $u$  through a torus  $(S^1)^n$  can be of constant rank. In this way, torus knots are more naturally studied through the lens of constant rank factorisations. The next example emphasises this difference a bit more starkly by exhibiting function that is like a torus knot but has no nontrivial quasiperiodic factorisations. The key idea is to violate the periodicity hypotheses of Proposition 5.

**Example 1.** The function  $u : \mathbb{R} \rightarrow \mathbb{R}$  given by:

$$u(x) := \sin x + \sin(\pi x)$$

has a constant rank factorisation:



where

$$\phi(x) := ([x]_{2\pi}, [\pi x]_{2\pi}), \tag{3.1}$$

and

$$U(y, z) := \sin y + \sin z,$$

since the derivative of  $\phi$  is a constant, hence of constant rank. Since the dimension of  $\mathbb{R}$  is 1, it follows that  $\phi$  cannot be a submersion  $\phi : \mathbb{R} \rightarrow (S^1 \times S^1)$  since the codomain is of dimension 2. (The reader is reminded that although  $\phi$  looks a bit like a torus knot, it is not, since the domain is  $\mathbb{R}$ . Moreover,  $\phi$  is not surjective, so it does not contradict the dimension bounds provided by the constant rank assumption.)

On the other hand,  $u$  has no quasiperiodic factorisation with  $S^1$  as the phase space, and so only has the trivial quasiperiodic factorisation. To see this, recall the trigonometric identity

$$\begin{aligned}
 \sin(x + y) \cos(x - y) &= \frac{1}{4i} (e^{i(x+y)} - e^{-i(x+y)}) (e^{i(x-y)} + e^{-i(x-y)}) \\
 &= \frac{1}{4i} (e^{2ix} - e^{-2ix} + e^{2iy} - e^{-2iy}) \\
 &= \frac{1}{2} \sin(2x) + \frac{1}{2} \sin(2y).
 \end{aligned}$$

Thus,

$$u(x) = 2 \sin\left(\left(\frac{1 + \pi}{2}\right)x\right) \cos\left(\left(\frac{1 - \pi}{2}\right)x\right).$$

The supremum of this function is certainly not more than 2, and its infimum is certainly not less than  $-2$ . It is a commonly recognised fact that the image of  $\phi : \mathbb{R} \rightarrow (S^1 \times S^1)$  given as Equation (3.1) is dense in  $S^1 \times S^1$ , so this means that the supremum of  $u$  is therefore equal to 2 and the infimum is equal to  $-2$ .

Now suppose that there was a quasiperiodic factorisation  $u = V \circ \psi$  with phase space  $S^1$  so that  $\psi : \mathbb{R} \rightarrow S^1$  and  $V : S^1 \rightarrow \mathbb{R}$ . Since  $S^1$  is compact,  $V$  must attain its maximum value, which must be 2,

and likewise  $V$  must attain its minimum value, which must be  $-2$ . Therefore, at the maximum,  $x$  must satisfy the equation:

$$2 = 2 \sin \left( \left( \frac{1 + \pi}{2} \right) x \right) \cos \left( \left( \frac{1 - \pi}{2} \right) x \right).$$

This means that

$$\left( \frac{1 + \pi}{2} \right) x = \left( \frac{1}{2} + 2n \right) \pi, \text{ and } \left( \frac{1 - \pi}{2} \right) x = 2m\pi$$

for some integers  $m$  and  $n$ . Therefore,

$$x = \frac{4m\pi}{1 - \pi}$$

so that

$$\frac{1 + 4n}{1 + \pi} = \frac{4m}{1 - \pi}.$$

Solving for  $m$ , we have that

$$m = \frac{1}{4} \left( \frac{1 - \pi}{1 + \pi} \right) (1 + 4n),$$

which is a contradiction since that quantity is not rational!

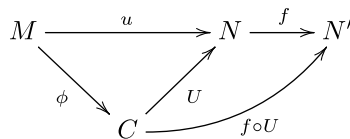
Taken together, Propositions 3 and 7 imply that any final object  $u = U \circ \phi$  of  $\mathbf{QuasiP}(u)$  is an object of  $\mathbf{Const}(u)$ . One therefore might speculate – in defiance of Proposition 7 – that  $u$  would also be a final object of  $\mathbf{Const}(u)$  as well. The map in Example 1 is a counterexample to this, however! Specifically, take an object of  $\mathbf{Const}(u)$  with a compact phase space (namely  $S^1 \times S^1$ ). There can be no  $\mathbf{Const}(u)$  morphism from this object to the single isomorphism class of  $\mathbf{QuasiP}(u)$ , since the phase space in that case is not compact; this is precluded by the constant rank assumption since it would violate Corollary 1.

### 3.1. Functoriality

The categories  $\mathbf{Const}(u)$  and  $\mathbf{QuasiP}(u)$  are natural in the sense that they are transformed functorially by pre- and post-composition of  $u$  with other smooth functions. The following Propositions are modifications of Theorem 1.

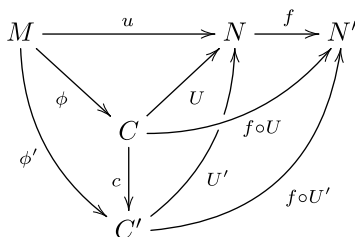
**Proposition 8.** *Suppose that  $u : M \rightarrow N$  and  $f : N \rightarrow N'$  are smooth maps. The map  $f$  induces a covariant functor  $\mathbf{QuasiP}(u) \rightarrow \mathbf{QuasiP}(f \circ u)$  and a covariant functor  $\mathbf{Const}(u) \rightarrow \mathbf{Const}(f \circ u)$ .*

*Proof.* Suppose  $u = U \circ \phi$  is a quasiperiodic or a constant rank factorisation in which  $C$  is the phase space. Then the following diagram commutes



which means that  $(f \circ u) = (f \circ U) \circ \phi$  is a factorisation of the same type as for  $u$ . This transforms the objects of the categories  $\mathbf{QuasiP}(u)$  or  $\mathbf{Const}(u)$ .

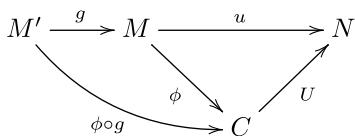
Morphisms are transformed in much the same way as objects, by composing  $f$  on the left, as can be seen from the commutative diagram:



Composition of morphisms is completely unchanged by this recipe, as it consists of composition of the maps on the phase space. □

**Proposition 9.** *Suppose that  $u : M \rightarrow N$  is a smooth map. If  $g : M' \rightarrow M$  is a surjective submersion, then  $g$  induces a covariant functor  $\mathbf{QuasiP}(u) \rightarrow \mathbf{QuasiP}(u \circ g)$ . Similarly, if  $g : M' \rightarrow M$  is a constant rank map, then  $g$  induces a covariant functor  $\mathbf{Const}(u) \rightarrow \mathbf{Const}(u \circ g)$ .*

*Proof.* Suppose  $u = U \circ \phi$  is a quasiperiodic factorisation in which  $C$  is the phase space. Because  $g$  is assumed to be a surjective submersion,  $(\phi \circ g)$  is also a surjective submersion. Therefore, the following diagram commutes



which means that  $(u \circ g) = U \circ (\phi \circ g)$  is a quasiperiodic factorisation. Similarly, if  $u = U \circ \phi$  is a constant rank factorisation, then under the assumption that  $g$  is a constant rank function, then so is  $(\phi \circ g)$ . This transforms the objects of the categories  $\mathbf{QuasiP}(u)$  or  $\mathbf{Const}(u)$ . Morphisms and their composition follow along *mutatis mutandis* as in the proof of Proposition 8. □

### 3.2. Functions with circular domains

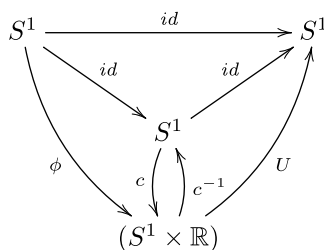
At present, the most complete characterisation of  $\mathbf{QuasiP}(u)$  that is known is Theorem 2, which is proven in this section. Theorem 2 applies when the domain  $M$  is the circle  $S^1$ . This characterisation relies on the observation that  $u$  becomes a loop in  $N$  and therefore has a representative  $[u]$  in the fundamental group  $\pi_1(N)$ .

**Example 2.** *Let us consider the identity map  $u = id_{S^1} : S^1 \rightarrow S^1$  and its category  $\mathbf{QuasiP}(id_{S^1})$  of quasiperiodic factorisations. First of all, its factorisation  $u = u \circ u$  is the final object of  $\mathbf{QuasiP}(u)$ . While this seems a little trivial, suppose that we had some other quasiperiodic factorisation  $u = U \circ \phi$  with  $S^1$  as its phase space. If  $\phi$  is not injective, this means that  $U \circ \phi$  is not injective, which contradicts its factorisation since  $u$  is injective. On the other hand, suppose that  $\phi : S^1 \rightarrow S^1$  was not surjective. Let  $x \in S^1$  be outside the image of  $\phi$ . Since  $\phi$  is continuous, there is an open neighbourhood of  $x$  outside the image of  $\phi$ , which amounts to saying that the image of  $\phi$  is homeomorphic to a closed interval. Such a map  $\phi$  must therefore have critical points and therefore cannot have constant rank. Therefore,  $\phi$  must be bijective to participate in a quasiperiodic factorisation of  $u = U \circ \phi$ . Since  $\phi$  is of constant rank, it is therefore a local diffeomorphism; bijectivity assures that it is a diffeomorphism.*

*Also,  $u$  cannot have  $\mathbb{R}$  as the phase space of any of its quasiperiodic factorisations. Since  $S^1$  is compact, this would imply that the phase map  $S^1 \rightarrow \mathbb{R}$  has at least one local maximum, which is a critical point. This violates the constant rank assumption.*

*On the other hand, with constant rank factorisations, there are many other possible phase spaces. Perhaps the easiest such is to take the cylinder  $S^1 \times \mathbb{R}$  as the phase space, with  $\phi(x) = (x, 0)$  and  $U(x, y) = x$ . It is clear that  $\phi$  is of constant rank (it is 1), and since the second factor in the cylinder is ignored, this assures that  $u = U \circ \phi$ . This factorisation is not isomorphic to the trivial one in*

**Const**( $u$ ), because that would imply the existence of a smooth, bijective map  $c : S^1 \rightarrow (S^1 \times \mathbb{R})$  such that the diagram below commutes



Such is evidently impossible on several grounds, the most damning of which is the classical invariance of dimension because  $S^1$  and  $S^1 \times \mathbb{R}$  are of differing dimension.

The above example illuminates a general principle about quasiperiodic factorisations whose domain is a circle.

**Lemma 2.** Every quasiperiodic factorisation of a smooth map  $u : S^1 \rightarrow N$  has either  $S^1$  or the single-point space as its phase space.

This does not hold for constant rank factorisations, since the phase map need not be surjective in that case.

*Proof.* If  $u = U \circ \phi$  is a quasiperiodic factorisation, this means that  $\phi$  is a surjective submersion. Therefore, the only options for the phase space are 0- or 1-dimensional. Additionally, because  $\phi$  is continuous and  $S^1$  is connected and compact, the phase space must also be connected and compact. One option is evidently the single-point space. Setting this aside, there are only two compact one-dimensional manifolds (with or without boundary), namely a closed interval or  $S^1$ . Any smooth map  $\phi$  from  $S^1$  to the closed interval must have at least one critical point, since the interval can be totally ordered and thus a maximum value is attained via compactness. The presence of critical points violates the requirement that  $\phi$  be a submersion, which leaves  $S^1$  as the only possible 1-dimensional phase space.  $\square$

Recall that since  $H_1(S^1) \cong \mathbb{Z}$ , every continuous map  $u : S^1 \rightarrow S^1$  induces a group homomorphism  $u_* : H_1(S^1) \rightarrow H_1(S^1)$  of the form:

$$u_*(n) = kn$$

for some integer  $k$ . We call  $k$  the degree  $deg(u)$  of  $u$ .

**Lemma 3.** (Standard; see [28, Sec. 2.2], for instance) If  $u, u_1, u_2 : S^1 \rightarrow S^1$  are smooth maps such that  $u = u_2 \circ u_1$ , then  $deg(u) = deg(u_2)deg(u_1)$ .

*Proof.* Consider the map  $u_* : H_1(S^1) \rightarrow H_1(S^1)$  induced by  $u$  on  $H_1(S^1)$ . We have that  $u_*([z]) = deg(u)[z]$  where  $[z]$  is the generator of  $H_1(S^1) \cong \mathbb{Z}$ . But since homology is functorial, we have that  $(u_2 \circ u_1)_*([z]) = (u_2)_*(u_1)_*([z]) = deg(u_2)deg(u_1)[z]$ .  $\square$

Another way to see that Lemma 3 is true is to recall that the prototypical map of degree  $n$  is  $z^n : \mathbb{C} \rightarrow \mathbb{C}$  in the complex plane, and composition of this with  $z^m$  yields  $(z^n)^m = z^{nm}$ .

Taking Lemma 2 to its next logical step, if  $U \circ \phi$  is a quasiperiodic factorisation of  $u : S^1 \rightarrow N$ , then  $\phi : S^1 \rightarrow S^1$  has a well-defined degree  $deg(\phi)$ . A useful consequence of Lemma 3 is that degrees characterise isomorphism classes of **QuasiP**( $u$ ) up to sign changes in some cases.

**Lemma 4.** Two quasiperiodic factorisations  $U_1 \circ \phi_1$  and  $U_2 \circ \phi_2$  of a smooth map  $u : S^1 \rightarrow N$  are isomorphic in **QuasiP**( $u$ ) if and only if  $|deg(\phi_1)| = |deg(\phi_2)|$ .

*Proof.* Suppose that we have two such factorisations  $u = U_1 \circ \phi_1 = U_2 \circ \phi_2$  which correspond to isomorphic objects of  $\mathbf{QuasiP}(u)$ . This means that we have a continuous map  $f$  such that the diagram commutes

$$\begin{array}{ccc}
 & S^1 & \\
 \phi_1 \nearrow & \uparrow & \searrow U_1 \\
 S^1 & & N \\
 \phi_2 \searrow & \downarrow & \nearrow U_2 \\
 & S^1 & 
 \end{array}
 \begin{array}{c}
 \uparrow f^{-1} \\
 \downarrow f
 \end{array}
 \tag{3.2}$$

In particular, this implies that  $\phi_2 = f \circ \phi_1$  and  $\phi_1 = f^{-1} \circ \phi_2$ . In terms of degrees, this means that  $\deg(\phi_2) = \deg(f)\deg(\phi_1)$  and  $\deg(\phi_1) = \deg(f^{-1})\deg(\phi_2)$ . Since all of these degrees must be non-zero integers, we have to conclude that  $\deg(f) = \deg(f^{-1}) = \pm 1$ , namely that  $|\deg(\phi_1)| = |\deg(\phi_2)|$ .

Conversely, suppose that we have two quasiperiodic factorisations  $u = U_1 \circ \phi_1 = U_2 \circ \phi_2$  with  $|\deg(\phi_1)| = |\deg(\phi_2)|$ . Does this imply the existence of a homeomorphism  $f$  such that the diagram in (3.2) commutes? Yes, the covering space classification theorem [28, Thm 1.38] yields an explicit construction of such a map  $f$ . Thus, the two quasiperiodic factorisations are isomorphic in  $\mathbf{QuasiP}(u)$ .  $\square$

The above Lemmas lead to the following characterisation of isomorphism classes of objects in  $\mathbf{QuasiP}(u)$ , at least when the domain of  $u$  is a circle.

**Theorem 2.** *If  $u : S^1 \rightarrow N$  is a smooth map, then the isomorphism classes of  $\mathbf{QuasiP}(u)$  are in bijective correspondence with cyclic subgroups of  $\pi_1(N)$  that contain  $[u]$ .*

*Proof.* First of all, if  $u$  is constant, then there is nothing to prove. Let us therefore assume that  $u$  is not constant for the remainder of the argument.

Suppose that  $u = U \circ \phi$  is a quasiperiodic factorisation. We will use this to generate a cyclic subgroup of  $\pi_1(N)$  that contains  $[u]$ . Because of Lemma 2,  $U : S^1 \rightarrow N$  therefore corresponds to an element  $[U] \in \pi_1(N)$ . Let  $T : \mathbf{Ob}(\mathbf{QuasiP}(u)) \rightarrow 2^{\pi_1(N)}$  be given by:

$$T(U \circ \phi) := \{[U]^k : k \in \mathbb{Z}\},$$

which is evidently a cyclic subgroup of  $\pi_1(N)$ . Moreover, Lemma 4 indicates that  $[u]$  is homotopic to  $[U]^{deg(\phi)}$ , and therefore  $T(U \circ \phi)$  contains  $[u]$  as required.

Suppose that  $H \subseteq \pi_1(N)$  is a cyclic subgroup containing  $[u]$ . That means that  $[u]$  is homotopic to  $[U]^k$  for some  $k$  and some  $U : S^1 \rightarrow N$ . We need to find a function  $\phi : S^1 \rightarrow S^1$  such that  $u = U \circ \phi$ . By the covering space classification theorem [28, Thm 1.38], one can construct such a  $\phi$  that additionally satisfies  $k = \deg(\phi)$ .

If two quasiperiodic factorisations of  $u = U_1 \circ \phi_1 = U_2 \circ \phi_2$  are  $\mathbf{QuasiP}(u)$ -isomorphic, then they generate the same cyclic subgroup of  $\pi_1(N)$ . To see this, note that  $|\deg(\phi_1)| = |\deg(\phi_2)|$  by Lemma 4, and therefore  $[u]$  is homotopic to both  $[U_1]^{deg(\phi_1)}$  and  $[U_2]^{deg(\phi_2)}$ . Since both are cyclic subgroups, this means that  $[U_1]^k$  and  $[U_2]^{\pm k}$  are homotopic so that  $T(U_1 \circ \phi_1)$  and  $T(U_2 \circ \phi_2)$  are the same subgroup.

Conversely, if two quasiperiodic factorisations of  $u = U_1 \circ \phi_1 = U_2 \circ \phi_2$  generate the same cyclic subgroup of  $\pi_1(N)$  via  $T$ , this means that  $\deg(\phi_1) = \pm \deg(\phi_2)$  and that  $[U_1]$  is homotopic to  $[U_2]$ . As a result of Lemma 4, these two factorisations are isomorphic in  $\mathbf{QuasiP}(u)$ .  $\square$

**Corollary 2.** *Suppose that  $u : S^1 \rightarrow S^1$  is a smooth map of degree  $n$ . Then the isomorphism classes of  $\mathbf{QuasiP}(u)$  are in bijective correspondence with the set of factors of  $|n|$ .*

*Proof.* First of all, isomorphism classes of  $\mathbf{QuasiP}(u)$  are characterised by Lemma 4. Secondly, by Lemma 3, any quasiperiodic factorisation into  $u = U \circ \phi$  will yield  $n = \deg(u) = \deg(U)\deg(\phi)$ .  $\square$

**Corollary 3.** *If  $u_1, u_2 : S^1 \rightarrow N$  are homotopic maps, then their categories  $\mathbf{QuasiP}(u_1)$  and  $\mathbf{QuasiP}(u_2)$  are equivalent.*

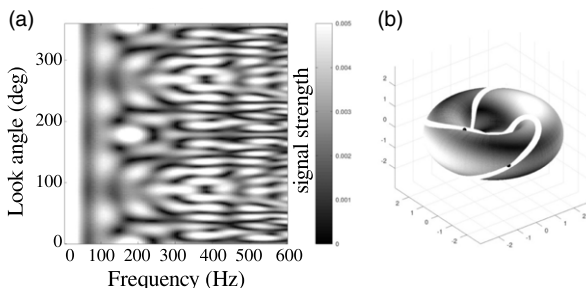


**Figure 10.** (a) Signature of the sum of a 4-fold symmetric scatterer and a 6-fold scatterer, (b) Response as a function of scatterer angles at 300 Hz.

### 3.3. Application: Factorisation categories of CSAS signatures

Let us revisit the CSAS example from Section 2. We remind the reader that for the purposes of this application, if we distort the sonar sensor’s trajectory there will be a distortion on both the look angle and the range. In the most general setting, both of these effects can be captured by the phase map  $\phi$ . In the specific case of CSAS echoes, the range distortion can be removed easily by time aligning each pulse separately, assuming the target has a large enough cross section. Therefore, we will assume that the trajectory distortions only apply to the look angle.

Consider the composite scatterer corresponding to a (2, 3) torus knot shown in Figure 6. There are many other composite scatterers with the same image in the torus. For instance, if we use  $P = 4$  and  $Q = 6$  in equations (2.2) and (2.3), we obtain a (4, 6) torus knot signature shown in Figure 10. The image of the path (though not the path itself) in the torus is shown in Figure 10(b) and is the same as that of the (2, 3) torus knot shown in Figure 7(a).

We can use Theorem 2 to compare these two signatures, and it is the case that they can be distinguished by their corresponding **QuasiP** categories. Notice that the torus has fundamental group  $\pi_1(S^1 \times S^1) = \mathbb{Z} \times \mathbb{Z}$ . There are two cyclic subgroups of  $\pi_1(S^1 \times S^1)$  that contain the (4, 6) torus knot, namely itself and the cyclic subgroup generated by the (2, 3) torus knot. On the other hand, there is only one cyclic subgroup of  $\pi_1(S^1 \times S^1)$  that contains the (2, 3) torus knot. Thus, the **QuasiP** categories of the (2, 3) and (4, 6) torus knots differ, and so there is no trajectory distortion that will transform one CSAS signature into the other. We can therefore conclude that they must be different targets.

## 4. Comparing functions via common factors

Being apparently topological in nature, one might imagine that if  $u_1, u_2 : M \rightarrow N$  are homotopic maps, then their categories **QuasiP**( $u_1$ ) and **QuasiP**( $u_2$ ) should be equivalent. This turns out to be false, the results of Section 3.2 (and Corollary 3 in particular) notwithstanding. This section presents two counterexamples to the equivalence of homotopy and the factorisation categories. Taken together, these two counterexamples establish that **QuasiP** is a topological invariant distinct from homotopy.

Given that the constructions of **QuasiP** and **Const** were motivated by the needs of sonar signatures, this means that the topological information inherent in sonar signatures is not entirely captured by homotopy equivalence classes for spaces of echoes. On the other hand, homotopy equivalence classes and equivalence classes of **QuasiP** and **Const** categories are related, as will be explored in subsequent sections of this article.

**Example 3.** Consider  $u_1, u_2 : [0, 1] \rightarrow [0, 1]$  in which  $u_1 = 0$  and  $u_2 = id$ . These two maps are evidently homotopic since  $h : [0, 1] \times [0, 1] \rightarrow [0, 1]$  given by:

$$h(x, t) := tx$$

is a smooth homotopy between them. Since  $u_2$  has rank 1, this means that any quasiperiodic factorisation of it  $u_2 = U \circ \phi$  must be a factorisation into two rank 1 functions. This effectively means that there is precisely one choice of phase space up to diffeomorphism, and consequently  $\text{QuasiP}(u_2)$  contains exactly one isomorphism class. On the other hand,  $u_1$  need not factor into two rank 1 functions; indeed the rank of  $\phi$  may be 0 or 1. Therefore,  $\text{QuasiP}(u_1)$  has two isomorphism classes.

Having equivalent categories of factorisations does not imply that two maps are homotopic, either.

**Example 4.** Consider the identity map  $u : S^1 \rightarrow S^1$  and the antipodal map  $(-u) : S^1 \rightarrow S^1$ . The maps  $u$  and  $(-u)$  have equivalent categories of quasiperiodic factorisations, since both are their own universal quasiperiodic factorisations (a consequence of [47, Thm. 8]), but they are not homotopic maps.

The net effect of these two examples is that  $\text{QuasiP}(u)$  is a topological invariant of a smooth map  $u : M \rightarrow N$  that is distinct from the homotopy class of  $u$ . There is still a somewhat more subtle relationship between homotopies and constant rank factorisation categories.

### 4.1. Signature equivalence

If we interpret a constant rank factorisation of  $u = U \circ \phi$  as a model of a sonar collection, it is natural to treat  $\phi$  as representing the trajectory effects and  $U$  as representing the target effects. To solve a sonar classification problem, all that matters is the signature: the  $U$  function. Two distinct sonar collections  $u_1 = U \circ \phi_1$  and  $u_2 = U \circ \phi_2$  with identical signatures should therefore be considered equivalent for the purposes of classification. We capture this idea with a definition of *signature equivalence* for factorisations. This section explores what properties are entailed when two collections have equivalent signatures.

**Definition 6.** If  $u_1 = U \circ \phi_1$  and  $u_2 = U \circ \phi_2$  are quasiperiodic factorisations such that the diagram

$$\begin{array}{ccc}
 M_1 & & \\
 \phi_1 \downarrow & \searrow^{u_1} & \\
 C & \xrightarrow{U} & N \\
 \phi_2 \uparrow & \swarrow_{u_2} & \\
 M_2 & & 
 \end{array} \tag{4.1}$$

commutes, we say that the factorisations of  $u_1$  and  $u_2$  have equivalent signatures. If instead of quasiperiodic factorisations in the diagram (4.1), we chose to use constant rank factorisations, then we say that the factorizations of  $u_1$  and  $u_2$  have constant rank equivalent signatures.

While equivalent signatures can also be thought of as a feature of the functions  $u_1$  and  $u_2$  (rather than the factorisations), constant rank signature equivalence becomes trivial when thought of this way (Proposition 13).

If  $u_1 = U \circ \phi_1$  and  $u_2 = U \circ \phi_2$  have equivalent signatures, one might think that the categories of quasiperiodic factorisations  $\text{QuasiP}(u_1)$  and  $\text{QuasiP}(u_2)$  are equivalent. This is not the case, as demonstrated by the next example.

**Example 5.** Consider  $M_1 = M_2 = N = S^1$ , the unit circle parameterised by an angle  $\theta$ . Suppose that

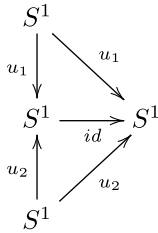
$$u_1(\theta) = 2\theta,$$

and

$$u_2(\theta) = 6\theta,$$

where we assume that angles outside the range  $[0, 2\pi)$  are wrapped back into that range. These functions have universal quasiperiodic factorisations with the same phase space,  $C = S^1$ , and  $U = id$  in both cases.

The diagram (4.1) becomes

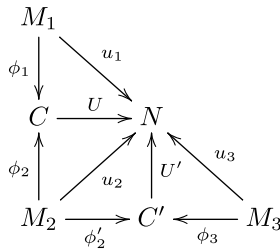


Thus, these two quasiperiodic factorisations have equivalent signatures, but according to Theorem 2, the categories  $\mathbf{QuasiP}(u_1)$  and  $\mathbf{QuasiP}(u_2)$  are not equivalent, because 2 is prime and 6 is composite.

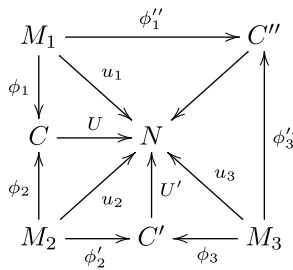
Calling a signature equivalence an *equivalence* is legitimate, because it is in fact an equivalence relation.

**Proposition 10.** Signature equivalence is an equivalence relation between two functions  $u_1, u_2 : M \rightarrow N$ . This remains true for constant rank signature equivalence.

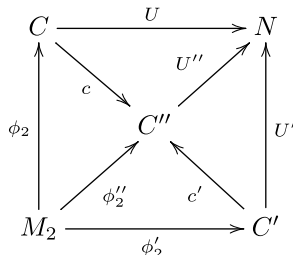
*Proof.* Symmetry is immediate from the definition. Reflexivity follows immediately upon recognising that every smooth function has a trivial quasiperiodic factorisation. To attempt to establish transitivity, the diagram we start with is



and what we want to construct is  $C''$  so that the diagram

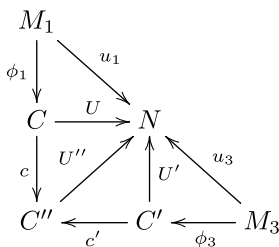


commutes with surjective submersions  $\phi''_1$  and  $\phi''_3$ . This can be accomplished by the unique final object in  $\mathbf{QuasiP}(u_2)$  according to Proposition 6 (or in  $\mathbf{Const}(u_2)$  according Proposition 7 in the case of constant rank factorisations), since this means that we can expand the corresponding portion of the diagram





to include such a factorisation of  $u_2 : M_2 \rightarrow N$  into  $U'' \circ \phi'_2$ . Composing maps from this diagram and the previous, we have the diagram



which we can use to define  $\phi'_1 = c \circ \phi_1$  and  $\phi'_3 = c' \circ \phi_3$ . That these two maps are surjective submersions is a consequence of [47, Lem. 14], which completes the argument.  $\square$

What do equivalence classes of signature equivalent functions look like? For one, all members of an equivalence class share the same image set. This provides a rather direct explanation of why classifying sonar targets using the persistent homology of the space of echoes is effective [49].

**Proposition 11.** *If  $u_1$  and  $u_2$  are signature equivalent functions, then they have identical image sets.*

This need not be true for constant rank signature equivalence.

*Proof.* Since  $u_1$  and  $u_2$  are signature equivalent, there is a pair of quasiperiodic factorisations,  $u_1 = U \circ \phi_1$  and  $u_2 = U \circ \phi_2$ , where  $U : C \rightarrow N$  for some space  $C$ . Suppose that  $y \in N$  is in the image of  $u_1$ , which means  $y$  is in the image of  $U$  as well. That means there is an  $x \in C$  such that  $U(x) = y$ . Since  $\phi_2$  is surjective by assumption,  $x$  is in the image of  $\phi_2$ , and hence there is a  $z$  for which  $u_2(z) = U(\phi_2(z)) = U(x) = y$ . This establishes that  $\text{image } u_2 \subseteq \text{image } u_1$ .

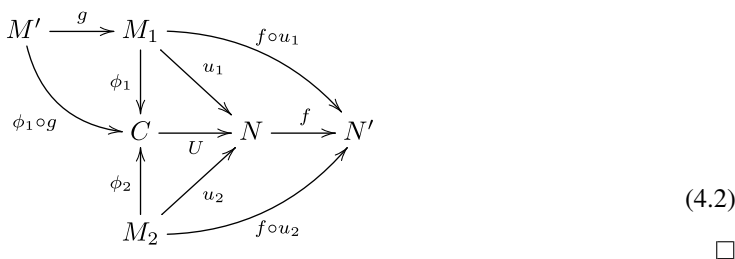
On the other hand, since  $\phi_1$  is also surjective by assumption, then a similar argument establishes that  $\text{image } u_1 \subseteq \text{image } u_2$ .  $\square$

Like the functoriality expressed in Propositions 8 and 9, (constant rank) signature equivalence respects pre- and post-composition with smooth functions.

**Proposition 12.** *Suppose that  $u_1 : M_1 \rightarrow N$  and  $u_2 : M_2 \rightarrow N$  have equivalent signatures.*

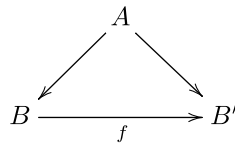
- (1) *If  $f : N \rightarrow N'$  is a smooth map, then  $(f \circ u_1)$  and  $(f \circ u_2)$  have equivalent signatures.*
- (2) *If  $g : M' \rightarrow M_1$  is a surjective submersion, then  $(u_1 \circ g)$  and  $u_2$  have equivalent signatures.*
- (3) *Statements (1) and (2) hold for constant rank versions, mutatis mutandis.*

*Proof.* All of the statements implied by this proposition follow from reasoning about a diagram of the form



Finally, although Example 5 shows that signature equivalence does not ensure that categories of quasiperiodic factorisations are equivalent, the categories are related in a more subtle way. Intuitively, the presence of a signature equivalence between two functions sets up an equivalence between subcategories within their respective categories of quasiperiodic factorisations. To state this precisely requires the notion of a *coslice category*.

**Definition 7.** (Standard) If  $A$  is an object of a category  $\mathbf{C}$ , the coslice category  $(A \downarrow \mathbf{C})$  contains every object  $B$  in  $\mathbf{C}$  for which there is a morphism  $A \rightarrow B$ . Morphisms of  $(A \downarrow \mathbf{C})$  consist of commuting diagrams of the form



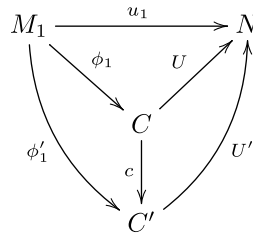
where  $f$  is a morphism of  $\mathbf{C}$ .

Briefly, the coslice category  $(A \downarrow \mathbf{C})$  is equivalent to the subcategory of  $\mathbf{C}$  generated by all morphisms and objects ‘downstream’ of  $A$ .

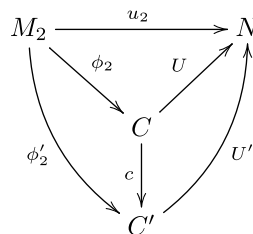
**Theorem 3.** Suppose that  $u_1 : M_1 \rightarrow N$  and  $u_2 : M_2 \rightarrow N$  are two maps with equivalent signatures. Suppose that we write the corresponding quasiperiodic factorisations  $u_1 = U \circ \phi_1$  and  $u_2 = U \circ \phi_2$ , respectively. Then the coslice categories  $(U \circ \phi_1 \downarrow \mathbf{QuasiP}(u_1))$  and  $(U \circ \phi_2 \downarrow \mathbf{QuasiP}(u_2))$  are isomorphic (not merely equivalent).

The proof of Theorem 3 relies upon an explicit construction of a functor between the coslice categories, the mechanics of which are explained in Lemma 5 below.

**Lemma 5.** Suppose that  $u_1 : M_1 \rightarrow N$  and  $u_2 : M_2 \rightarrow N$  are two maps with quasiperiodic factorisations  $u_1 = U \circ \phi_1$  and  $u_2 = U \circ \phi_2$ . If  $u_1 = U' \circ \phi'_1$  is another quasiperiodic factorisation of  $u_1$  such that there is a  $\mathbf{QuasiP}(u_1)$  morphism

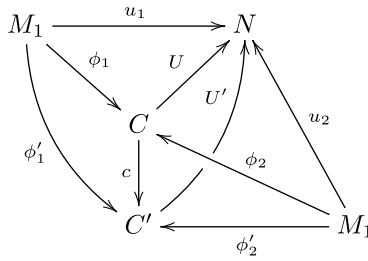


where  $c : C_1 \rightarrow C_2$  is a smooth map, then this induces another quasiperiodic factorisation of  $u_2 = U' \circ \phi'_2$  and a  $\mathbf{QuasiP}(u_2)$  morphism



The statement remains true of constant rank factorisations as well.

*Proof.* This Lemma hinges on the observation that  $\phi'_1 = c \circ \phi_1$ . We can then simply make the definition  $\phi'_2 = c \circ \phi_2$ , because all of the various paths in the diagram for  $u_2$



continue to commute. Notice that commutativity of the original morphism diagram ensures that  $c$  be a surjective submersion, so it follows that  $\phi'_2$  is also a surjective submersion. The statement still holds for constant rank maps for essentially the same reason: it follows from the definition of morphism that  $c$  must be a constant rank map.  $\square$

With Lemma 5 in hand, we can prove Theorem 3.

*Proof.* (of Theorem 3) Observe that Lemma 5 defines a function on objects:

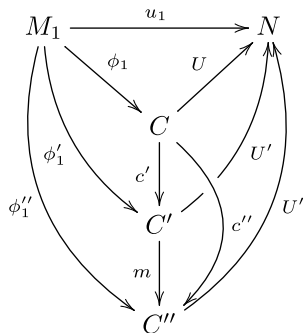
$$F : (U \circ \phi_1 \downarrow \mathbf{QuasiP}(u_1)) \rightarrow (U \circ \phi_2 \downarrow \mathbf{QuasiP}(u_2)).$$

Dually, the same construction works to define a function:

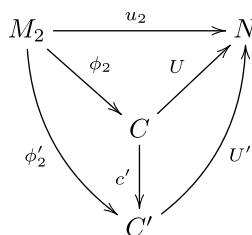
$$G : (U \circ \phi_2 \downarrow \mathbf{QuasiP}(u_2)) \rightarrow (U \circ \phi_1 \downarrow \mathbf{QuasiP}(u_1)).$$

We need to establish that (1)  $F$  respects morphisms and therefore defines a covariant functor, (2) that  $F \circ G = \text{id}$ , and that (3)  $G \circ F = \text{id}$ . Evidently due to the symmetry of the situation, (2) and (3) can be established simultaneously.

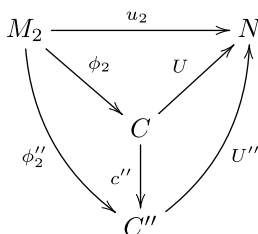
Suppose that we have a morphism  $m : (\phi'_1, U') \rightarrow (\phi'_1, U'')$  in  $(U \circ \phi_1 \downarrow \mathbf{QuasiP}(u_1))$ , which means that the following diagram commutes



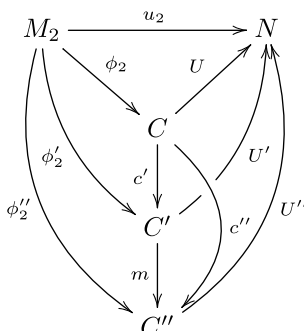
where  $c'$ ,  $c''$ , and  $m$  are smooth maps (abusing notation by conflating the morphisms with their component maps on the phase spaces). Notice in particular that  $c'' = m \circ c'$ . Lemma 5 uses the above to construct two diagrams for factorisations of  $u_2$ , namely



and



But since  $c'' = m \circ c'$ , these two diagrams can be combined into



which is the diagram of a morphism  $F(m) : (\phi'_2, U') \rightarrow (\phi'_2, U'')$  in  $(U \circ \phi_2 \downarrow \mathbf{QuasiP}(u_2))$ . Incidentally  $F(m)$  is also given by the smooth map  $m$  on the phase spaces.

To establish that  $F$  and  $G$  are inverses, it is merely necessary to compute using the recipe from Lemma 5:

$$\begin{aligned}
 G(F((\phi'_1, U'))) &= G(F((c \circ \phi_1, U'))) \\
 &= G((c \circ \phi_2, U')) \\
 &= (c \circ \phi_1, U') \\
 &= (\phi'_1, U')
 \end{aligned}$$

as desired. □

If the factorisations of two functions  $u_1$  and  $u_2$  are signature equivalent and are final elements in their respective categories, then their coslice categories are rather small and uninformative. Conversely (though trivially!), if the factorisations are the trivial ones, then this forces their respective categories to be isomorphic.

#### 4.2. Constant rank signature equivalences

Constant rank signature equivalences appear to have many of the same features of signature equivalences, since several of the proofs from the statements in Section 4 carry over to constant rank signature equivalences without much effort. However, constant rank signature equivalences are a relatively coarse way of comparing two functions, because there are simply too many of them, as will be shown in Proposition 13. Intuitively, this means that sonar signatures arising in this case have too many degrees of freedom to be effectively discriminated. This is a bit disappointing because constant rank signature equivalences are closely related to homotopies (as will be shown in Proposition 14) even though signature equivalences are not. The solution appears in Definition 8. Instead of considering individual equivalences, we should consider a category of *all possible such* constant rank equivalences. This

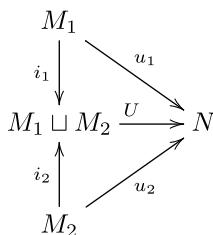
idea builds over the next few sections, culminating in Theorem 5, which characterises the category of constant rank equivalences in terms of coslices.

A close examination reveals that none of the arguments in the proof of Theorem 3 were dependent on the surjectivity of the phase maps. Therefore, we have the following Corollary.

**Corollary 4.** *Suppose that  $u_1 : M_1 \rightarrow N$  and  $u_2 : M_2 \rightarrow N$  are two maps with constant rank factorisations  $u_1 = U \circ \phi_1$  and  $u_2 = U \circ \phi_2$  being constant rank signature equivalent factorisations. Then the coslice categories  $(U \circ \phi_1 \downarrow \mathbf{Const}(u_1))$  and  $(U \circ \phi_2 \downarrow \mathbf{Const}(u_2))$  are isomorphic (not merely equivalent).*

Constant rank signature equivalences always exist between functions, at least in a trivial form, as the next Proposition shows.

**Proposition 13.** *Suppose that  $u_1 : M_1 \rightarrow N$  and  $u_2 : M_2 \rightarrow N$  are two smooth functions. Recalling that  $M_1 \sqcup M_2$  is the disjoint union of the two manifolds involved, then*



is a constant rank signature equivalence when the vertical  $i_k$  maps are inclusions and

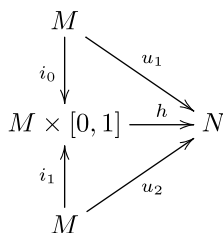
$$U(x) = \begin{cases} u_1(x) & \text{if } x \in M_1 \subseteq M_1 \sqcup M_2, \\ u_2(x) & \text{if } x \in M_2 \subseteq M_1 \sqcup M_2. \end{cases}$$

*Proof.* One merely needs to recognise that the diagram commutes by construction, and that inclusions are automatically constant rank maps. □

The reader is cautioned from reading too much into Proposition 13. Because of Proposition 4, neither of the constant rank factorisations in Proposition 13 are initial objects in their categories of constant rank factorisations. If the factorizations in Proposition 13 were initial objects in general, then Corollary 4 would indicate that  $\mathbf{Const}(u)$  is dependent *only* on the codomain of  $u$ . The truth is quite a bit more subtle!

**Proposition 14.** *Suppose that  $u_1, u_2 : M \rightarrow N$  are two maps and that  $h : M \times [0, 1] \rightarrow N$  is a smooth homotopy between them. Then these maps are constant rank signature equivalent.*

*Proof.* The hypothesis means that



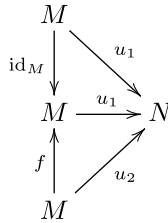
commutes. Furthermore,  $u_1 = h \circ i_0$  and  $u_2 = h \circ i_1$  are both constant rank factorisations.<sup>5</sup> □

Therefore, the constant rank signature equivalence classes contain entire homotopy classes of maps.

<sup>5</sup>Neither are surjective, so this does not result in quasiperiodic factorisations.

**Proposition 15.** *Suppose  $M$  is a connected manifold, that  $u_1, u_2 : M \rightarrow N$  are smooth maps, and that  $u_2 = u_1 \circ f$  where  $f : M \rightarrow M$  is a diffeomorphism. Then these maps are constant rank signature equivalent.*

*Proof.* The hypothesis establishes that



commutes; evidently  $f$  and  $\text{id}_M$  are of constant rank. □

Using Proposition 15 to establish a constant rank signature equivalence along with Corollary 4 provides an alternative proof of Theorem 1, since the factorisations in question are evidently initial according to Proposition 4.

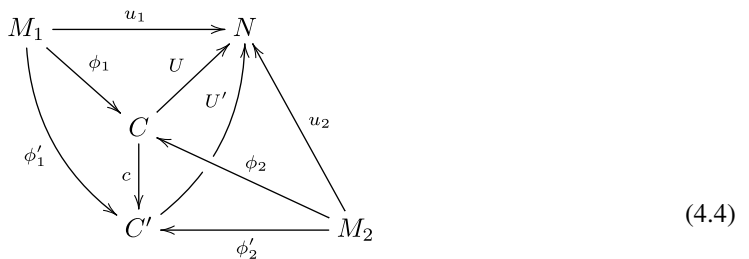
**4.3. Categories of signature equivalences**

The fact that constant rank signature equivalences are so common suggests that we abstract further and consider these equivalences as objects in their own right.

**Definition 8.** *The category  $\text{CRSE}(u_1, u_2)$  for each pair of smooth functions  $u_1 : M_1 \rightarrow N, u_2 : M_2 \rightarrow N$  has constant rank signature equivalences as its objects. Specifically, the objects are diagrams of the form:*



in which  $\phi_1$  and  $\phi_2$  are constant rank maps. A morphism in  $\text{CRSE}(u_1, u_2)$  is determined by a map  $c : C \rightarrow C'$  such that the diagram

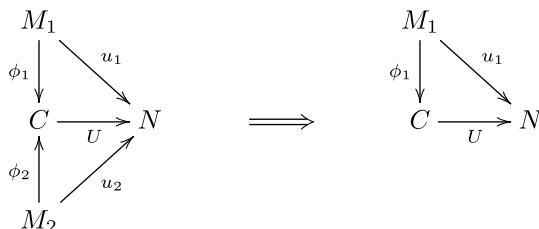


commutes.

Intuitively, each object of  $\text{CRSE}(u_1, u_2)$  defined above is an individual sonar target that could have yielded both signals  $u_1$  and  $u_2$  under different sensor conditions. Therefore, a small number of

isomorphism classes of  $\mathbf{CRSE}(u_1, u_2)$  suggests that  $u_1$  and  $u_2$  are likely from different targets, while a larger number of isomorphism classes means that it is likely that  $u_1$  and  $u_2$  arise from similar targets.

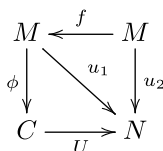
**Corollary 5.** *There is a forgetful functor  $\mathbf{CRSE}(u_1, u_2) \rightarrow \mathbf{Const}(u_1)$  that acts by truncating the diagram on the left to produce the one on the right:*



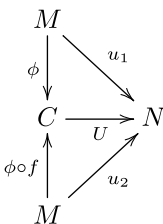
Evidently there is also a forgetful functor  $\mathbf{CRSE}(u_1, u_2) \rightarrow \mathbf{Const}(u_2)$  that acts by truncating the top portion of the diagram instead.

**Theorem 4.** *Suppose that  $u_1$  and  $u_2$  are smooth maps  $M \rightarrow N$  for a connected manifold  $M$ , and that  $u_2 = u_1 \circ f$  for some diffeomorphism  $f$ . Then the forgetful functors defined in Corollary 5 are surjective on objects (but not necessarily morphisms).*

*Proof.* Suppose that  $u_1 = U \circ \phi$  is a constant rank factorisation of  $u_1$ . By hypothesis, we therefore have the commutative diagram:



which can be rearranged as:

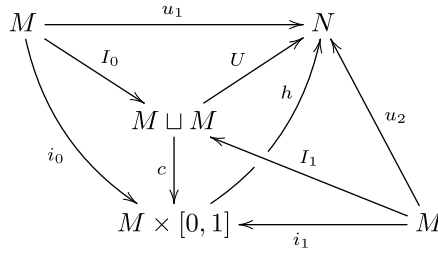


which is evidently an object in  $\mathbf{CRSE}(u_1, u_2)$  whose image through the forgetful functor is  $U \circ \phi$ . Repeating the argument using  $u_1 = u_2 \circ \phi^{-1}$  completes the proof.  $\square$

**Example 6.** *Let  $u_1 : \mathbb{R} \rightarrow \mathbb{R}$  be the constant map  $u_1(x) = 0$  and  $u_2 : \mathbb{R} \rightarrow \mathbb{R}$  be the identity map  $u_2(x) = x$ . The functor in Corollary 5 for  $\mathbf{CRSE}(u_1, u_2) \rightarrow \mathbf{Const}(u_1)$  is not surjective on objects. To see this, notice that the constant rank factorisation  $\mathbb{R} \rightarrow \star \rightarrow \mathbb{R}$  of  $u_1$  through the single-point space  $\star$  cannot be constant rank signature equivalent to any constant rank factorisation of  $u_2$  and thus must be outside the image of the functor.*

Taking Theorem 4 and Example 6 together, this gives a means for comparing two smooth maps  $u_1, u_2$ . If the images of  $\mathbf{CRSE}(u_1, u_2)$  in  $\mathbf{Const}(u_1)$  and  $\mathbf{Const}(u_2)$  are both large, then the maps are similar. Homotopies yield another, related notion of similarity between maps as the next example shows.

**Example 7.** *If  $u_1, u_2 : M \rightarrow N$  are homotopic smooth maps, then the combined effect of Propositions 13 and 14 is that there is a morphism in  $\mathbf{CRSE}(u_1, u_2)$  of the form:*



where the  $I_k$  and  $i_k$  maps are the obvious inclusions,  $U$  is defined as in Proposition 13, and

$$c(x) = \begin{cases} (x, 0) & \text{if } x \text{ is in the first copy of } M \\ (x, 1) & \text{if } x \text{ is in the second copy of } M. \end{cases}$$

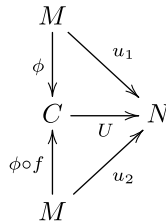
Given the definition of  $\mathbf{CRSE}(u_1, u_2)$ , it is easy to recast some of the previous results on functoriality.

**Proposition 16.** *Suppose that  $u_1 : M_1 \rightarrow N$ ,  $u_2 : M_2 \rightarrow N$  and  $f : N \rightarrow N'$  are smooth maps. Then  $f$  induces a covariant functor  $\mathbf{CRSE}(u_1, u_2) \rightarrow \mathbf{CRSE}(f \circ u_1, f \circ u_2)$  via the construction in statement (1) of Proposition 12.*

*Proof.* This follows from a tedious (but easy) diagram chase using the diagram in the proof of Proposition 12. Covariance is assured for the same reason as in Proposition 8. □

**Proposition 17.** *The constant rank signature equivalence constructed in Proposition 13 for  $u_1 : M_1 \rightarrow N$  and  $u_2 : M_2 \rightarrow N$  is the initial object of  $\mathbf{CRSE}(u_1, u_2)$ .*

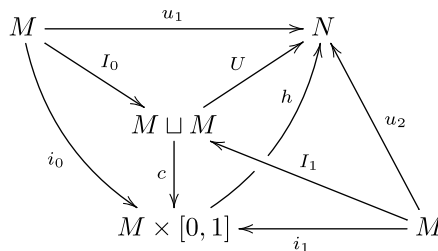
*Proof.* Suppose that we have an arbitrary object of  $\mathbf{CRSE}(u_1, u_2)$ , given by the diagram



Consider the map  $c : (M_1 \sqcup M_2) \rightarrow C$  given by:

$$c(x) = \begin{cases} \phi_1(x) & \text{if } x \in M_1 \subseteq M_1 \sqcup M_2 \\ \phi_2(x) & \text{if } x \in M_2 \subseteq M_1 \sqcup M_2 \end{cases}$$

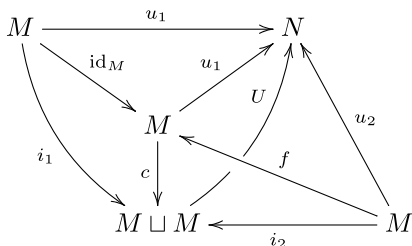
By construction, this map makes the diagram



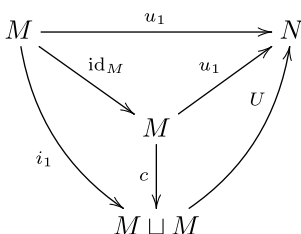
commute when the  $i_k$  maps are the inclusions. □



The initial objects of  $\mathbf{CRSE}(u_1, u_2)$  and that of  $\mathbf{Const}(u_1)$  are quite incompatible, even if there is a diffeomorphism  $u_2 = u_1 \circ f$ ! This is because there is no map  $c$  that will make the following diagram commute:



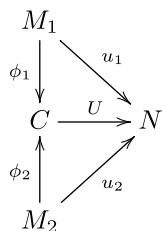
Moreover, considering the images of these objects of  $\mathbf{CRSE}(u_1, u_2)$  in  $\mathbf{Const}(u_1)$ , there is precisely one  $c$  that will make the following diagram commute:



Reversing the direction of the  $c$  maps in the above two diagrams yields exactly one possible option in the top diagram, and many options in the bottom one.

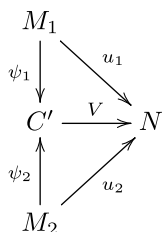
On the other hand, final objects of  $\mathbf{CRSE}(u_1, u_2)$  and  $\mathbf{Const}(u_1)$  are compatible. This should not come as a surprise because Proposition 7 asserts that every such final object has the same phase space—separable infinite-dimensional Hilbert space.

**Proposition 18.** *Suppose that*

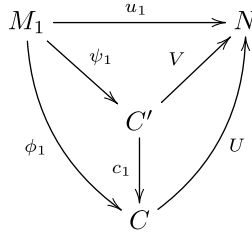


*is a constant rank signature equivalence and that  $u_1 = U \circ \phi_1$  and  $u_2 = U \circ \phi_2$  are final objects in  $\mathbf{Const}(u_1)$  and  $\mathbf{Const}(u_2)$ , respectively. Then their constant rank signature equivalence is final in  $\mathbf{CRSE}(u_1, u_2)$ .*

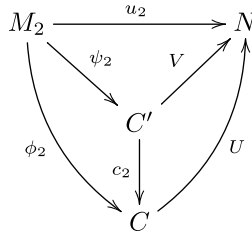
*Proof.* Suppose that



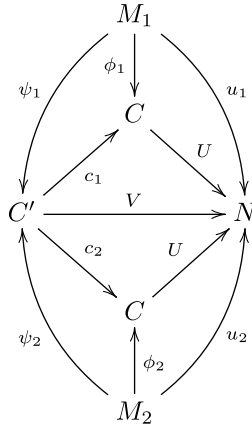
is another object of  $\mathbf{CRSE}(u_1, u_2)$ . Using the hypothesis that  $u_1 = U \circ \phi_1$  and  $u_2 = U \circ \phi_2$  are final objects, this implies that there is a  $\mathbf{Const}(u_1)$  morphism:



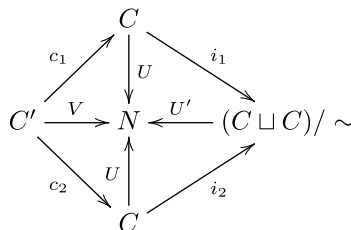
and a  $\mathbf{Const}(u_2)$  morphism



These can be assembled into a larger diagram

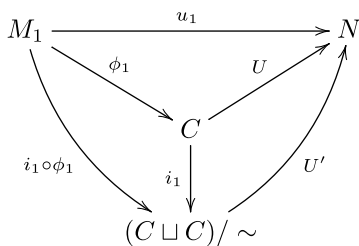


To complete the argument, we need to show that the two maps  $c_1, c_2$  can be replaced with a single map  $c : C' \rightarrow C$ , even though  $c_1$  and  $c_2$  might disagree. To that end, consider  $(C \sqcup C) / \sim$ , where  $x \sim y$  if there is a  $z \in C'$  such that  $c_1(z) = x$  and  $c_2(z) = y$ . This construction makes the diagram



commute if  $U'$  is given by  $U$  on both copies of  $C$  in  $(C \sqcup C) / \sim$ .

Splicing the two previous diagrams together yields the observation that there is a morphism



Applying finality in  $\mathbf{Const}(u_1)$  once more, we must conclude that the factorisation through  $(C \sqcup C) / \sim$  is  $\mathbf{Const}(u_1)$ -isomorphic to  $U \circ \phi_1$ . A similar argument holds for the other factorisation. Therefore, we must have that  $(C \sqcup C) / \sim$  is diffeomorphic to  $C$  so that  $c_1$  and  $c_2$  can only disagree up to that diffeomorphism.  $\square$

A consequence of Proposition 17 is a characterisation of  $\mathbf{CRSE}(u_1, u_2)$  in terms of coslice categories of  $\mathbf{Const}(u_1)$  and  $\mathbf{Const}(u_2)$ .

**Theorem 5.** *If  $u_1 : M_1 \rightarrow N$  and  $u_2 : M_2 \rightarrow N$  are two smooth maps,  $\mathbf{CRSE}(u_1, u_2)$  is isomorphic to the coslice category  $(U \circ i_1 \downarrow \mathbf{Const}(u_1))$  (and therefore also to the coslice category  $(U \circ i_2 \downarrow \mathbf{Const}(u_2))$ ), where  $U, i_1$ , and  $i_2$  are defined as in Proposition 13.*

*Proof.* Each object of  $\mathbf{CRSE}(u_1, u_2)$  already implies the existence of two constant rank factorisations:  $u_1 = U' \circ \phi_1$  and  $u_2 = U' \circ \phi_2$ .

According to Proposition 17, we have a  $\mathbf{CRSE}(u_1, u_2)$  morphism from  $(U \circ i_1, U \circ i_2)$  (the initial object) to  $(U' \circ \phi_1, U' \circ \phi_2)$  (an arbitrary object), implying the existence of corresponding morphisms in  $\mathbf{Const}(u_1)$  and  $\mathbf{Const}(u_2)$ . Consequently, this means that the factorisations  $u_1 = U' \circ \phi_1$  and  $u_2 = U' \circ \phi_2$  can be considered objects in the corresponding coslice categories. Conversely, the construction of the equivalence between the coslice categories involved in the proof of Theorem 3 is precisely the same construction as that for  $\mathbf{CRSE}(u_1, u_2)$ .  $\square$

#### 4.4. Application: Signature equivalence in CSAS

Recall the CSAS example of a 3-fold symmetric scatterer from Section 2. In that example, signatures from a 3-fold symmetric scatterer without distortions (Figure 3(b)) and with distortions (Figure 4(a)) were shown. Since they differ only by a smooth trajectory distortion, this is an example of a signature equivalence (Definition 4.1), since the phase maps are invertible.

Since they differ by a smooth trajectory distortion, which happens to be a diffeomorphism, Theorem 1 argues that the factorisation categories for these two signatures are isomorphic, not just equivalent, which means that there should be a bijective correspondence between their factorisations. Hence, Proposition 11 implies that their image sets should be identical. From a practical standpoint, this means that the set of possible echoes (rows) in Figures 3(b) and 4(a) should be identical. A good way to see this is to compare their principal components analysis plots, shown in Figure 11. In computing these plots, pairs of adjacent rows were used as coordinates for each pulse, and the axes (the principal vectors for Figure 3(b)) are the same for both plots. Adjacent rows were used as a proxy for the derivative of the phase function, which is of constant rank by Proposition 5. Notice that the two frames of Figure 11 show very similar trajectories; they only differ due to sampling effects because a finite number of pulses were used.

Leaving the scatterers fixed while changing the relative angle, changes the intercept of the trajectory along the torus. Equivalently, changing the relative angle simply shifts the underlying function on the torus, as Figures 12(a)–(b) show. These figures are therefore an example of constant rank signature equivalence. On the other hand, if the symmetry of the scatterers is changed, this dramatically changes the function and the torus knot, as shown in Figure 12(a) and (c).

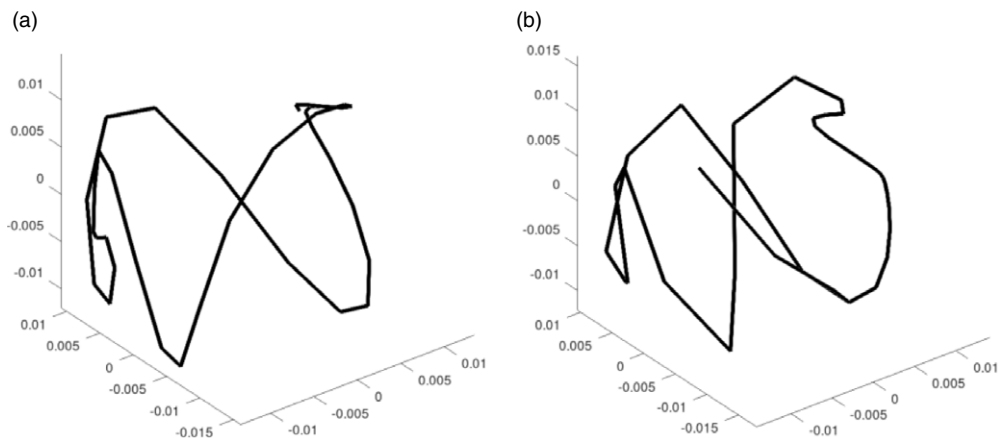


**Figure 11.** Principal components analysis plots of the signature of (a) a 3-fold symmetric scatterer (Figure 3(b)) and (b) a distorted 3-fold symmetric scatterer (Figure 4(a)).

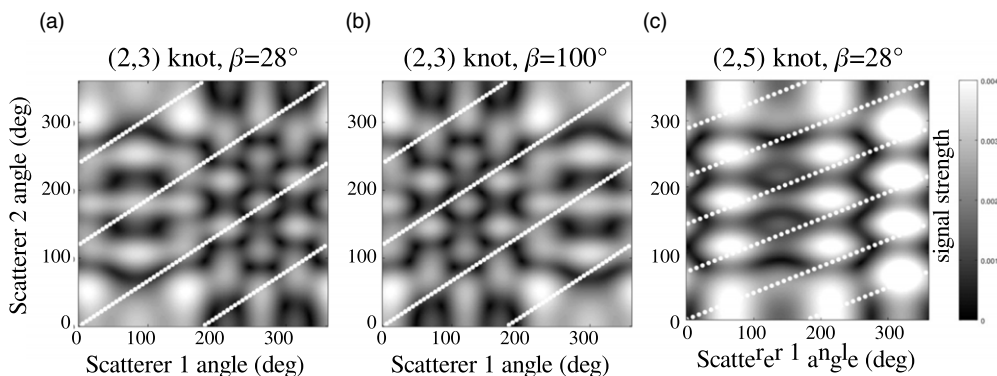


**Figure 12.** Different responses at 300 Hz for (a) the (2, 3) torus knot signature with relative angle  $28^\circ$ , (b) the (2, 3) torus knot signature with relative angle  $100^\circ$ , and (c) the (2, 5) torus knot signature with relative angle  $28^\circ$ .

Two targets with the same symmetry class (which have isomorphic **Const** categories), as in Figure 12(a)–(b), can be discriminated by constant rank signature equivalence since that is a generalisation of comparing the values of their signatures on a fundamental domain. In the case of changing the relative angles, these two targets are constant rank signature equivalent. Figure 12(a) and (c) are not constant rank signature equivalent, since the torus functions (signatures) are different. Evidently, classifying *all* constant rank signature equivalences would involve classifying all functions on the torus. This is not particularly easy to do completely, even though it is easy to identify when two such functions are equal.

## 5. Conclusion

This article has provided a nearly complete answer as to why topological methods are effective at solving sonar classification problems. Specifically, topological methods decouple trajectory effects from

the classification-relevant information contained in a sonar signature. Because of this decoupling, topological methods can be used when trajectory information is inaccurate or missing.

In answering the practical challenge of understanding sonar classification, this article has defined several new topological invariants that apply to factorisations of smooth functions and has established key properties about them. In the case of the category **QuasiP**, we have a complete characterisation in the case that applies to CSAS classification problems. This characterisation relies on the computation of the fundamental group of the space of echoes, which can be estimated from sonar data using persistent homology. Therefore, this article has provided theoretical justification for what was demonstrated experimentally in [49].

Given the fact that several new invariants were discovered, much work still remains. Although we understand how to compute the **QuasiP** category in some cases, we have only a very limited understanding of how to characterise the related category **Const**. The techniques that are effective for **QuasiP** are simply uninformative for **Const**. Additionally, the complete characterisation of **QuasiP** only applies to a limited class of synthetic aperture problems, so further work to characterise it under arbitrary sonar collections still remains.

**Acknowledgements.** The author would like to thank the anonymous referee for useful suggestions that have improved the quality of the exposition. This article is based on work supported by the Office of Naval Research (ONR) under Contract Nos. N00014-15-1-2090, N00014-18-1-2541 and N00014-22-1-2659. Any opinions, findings and conclusions or recommendations expressed in this article are those of the author and do not necessarily reflect the views of the Office of Naval Research.

**Conflict of interests.** None.

## References

- [1] Andén, J. & Mallat, S. (2014) Deep scattering spectrum. *IEEE Trans. Signal Process.* **62**, 4114–4128.
- [2] Azimi-Sadjadi, M. R., Huang, Q. & Dobeck, G. J. (1998) Underwater target classification using multi-aspect fusion and neural networks. In: *Aerospace/Defense Sensing and Controls*, International Society for Optics and Photonics, pp. 334–341.
- [3] Azimi-Sadjadi, M. R., Yao, v., Huang, Q. & Dobeck, G. J. (2000) Underwater target classification using wavelet packets and neural networks. *IEEE Trans. Neural Networks* **11**(3), 784–794.
- [4] Bonifant, W. W., Richards, M. A. & McClellan, J. H. (1999) An analysis of the effect of motion and phase errors on the implementation of interferometric processing by synthetic aperture sonar. In: *Conference Record of the Thirty-Third Asilomar Conference on Signals, Systems, and Computers (Cat. No.CH37020)*, Vol. 1, pp. 269–273.
- [5] Bruna, J. & Mallat, S. (2013) Invariant scattering convolution networks. *IEEE Trans. Pattern Anal. Mach. Intell.* **35**, 1872–1886.
- [6] Bucaro, J. A., Houston, B. H., Simpson, H., Saniga, M. & Sarkissian, A. (2010) Wide area detection and identification of underwater UXO using structural acoustic sensors. Technical Report Technical Report NRL/MR/7130–11-9337, Naval Research Laboratory.
- [7] Bucaro, J. A., Waters, Z. J., Houston, B. H., Simpson, H. J., Sarkissian, A., Dey, S. & Yoder, T. J. (2012) Acoustic identification of buried underwater unexploded ordnance using a numerically trained classifier. *J. Acoust. Soc. Am.* **132**(6), 3614–3617.
- [8] Carin, L., Dasgupta, N. & Haron, S. (2006) Progress report on development of algorithms for low-frequency sonar sensing. Technical report, Signal Innovations Group.
- [9] Carin, L., Liu, H., Yoder, T., Couchman, L., Houston, B. & Bucaro, J. (2004) Wideband time-reversal imaging of an elastic target in an acoustic waveguide. *J. Acoust. Soc. Am.* **115**(1), 259–268.
- [10] Carpenter, G. A. & Streilein, W. W. (1998) Artmap-ftr: a neural network for fusion target recognition with application to sonar classification. In: *Aerospace/Defense Sensing and Controls*, International Society for Optics and Photonics, pp. 342–356.
- [11] Chambers, D. H. (2007) Target characterization using time-reversal symmetry of wave propagation. *Int. J. Modern Phys. B* **21**(20), 3511–3555.
- [12] Chen, C., Ni, X., Bai, Q. & Wang, Y. (2019) A topological regularizer for classifiers via persistent homology. In: *AISTATS*.
- [13] Chen, J. L. & Summers, J. E. (2016) Deep neural networks for learning classification features and generative models from synthetic aperture sonar big data. *J. Acoust. Soc. Am.* **140**, 3423–3423.
- [14] Chen, S. & Wang, Y. (2021) Approximation algorithms for 1-Wasserstein distance between persistence diagrams. arxiv:2104.07710.
- [15] Chevillon, D., Rastello, T. & Vray, D. (1998) A fourier-based motion estimation approach for wide band synthetic aperture sonar. In: *IEEE Oceanic Engineering Society. OCEANS'98. Conference Proceedings (Cat. No.98CH36259)*, Vol. 3, pp. 1671–1675.

- [16] Cotter, E., Joslin, J. & Polagye, B. L. (2018) Tracking and classification of targets detected by a moving multibeam sonar. *J. Acoust. Soc. Am.* **143**, 1957–1957.
- [17] Dasgupta, N. & Carin, L. (2005) Time-reversal imaging for classification of submerged elastic targets via Gibbs sampling and the relevance vector machine. *J. Acoust. Soc. Am.* **117**(4), 1999–2011.
- [18] de Silva, V., Morozov, D. & Vejdemo-Johansson, M. (2011) Persistent cohomology and circular coordinates. *Discrete Comput. Geom.* **45**(4), 737–759.
- [19] Dey, T. K., Fan, F. & Wang, Y. (2014) Computing topological persistence for simplicial maps. In: *Proceedings of the Thirtieth Annual Symposium on Computational Geometry*.
- [20] Divyabarathi, G., Shailesh, S. & Judy, M. V. (2020) Survey on deep learning techniques used for classification of underwater sonar images. In: *GeographyRN: Nature-Society Studies (Topic)*.
- [21] Essl, G. (2020) Topological IIR filters over simplicial topologies via sheaves. *IEEE Signal Process. Lett.* **27**, 1215–1219.
- [22] Friedman, A. D., Mitchell, S. K., Kooij, T. L. & Scarbrough, K. N. (2005) Circular synthetic aperture sonar design. In: *Europe Oceans 2005*, Vol. 2, pp. 1038–1045.
- [23] Gaumont, C. F., Fromm, D. M., Lingeitch, J. F., Menis, R., Edelmann, G. F., Calvo, D. C. & Kim, E. (2006) Demonstration at sea of the decomposition-of-the-time-reversal-operator technique. *J. Acoust. Soc. Am.* **116**(2), 2574–A.
- [24] Goldblatt, R. (2006) *Topoi: The Categorical Analysis of Logic*, Dover, New York, USA.
- [25] Gorman, R. P. & Sejnowski, T. J. (1988) Analysis of hidden units in a layered network trained to classify sonar targets. *Neural Networks* **1**(1), 75–89.
- [26] Gruber, F. K., Marengo, E. A. & Devaney, A. J. (2004) Time-reversal imaging with multiple signal classification considering multiple scattering between the targets. *J. Acoust. Soc. Am.* **115**(6), 3042–3047.
- [27] Harker, S., Kokubu, H., Mischaikow, K. & Pilarczyk, P. (2016) Inducing a map on homology from a correspondence. *Proc. Am. Math. Soc.* **144**(4), 1787–1801.
- [28] Hatcher, A. (2002) *Algebraic Topology*, Cambridge University Press, Cambridge, UK.
- [29] Henderson, D. W. (1969) Infinite-dimensional manifolds are open subsets of hilbert space. *Bull. Amer. Math. Soc.* **75**(4), 759–762.
- [30] Hörmander, L. (1971) Fourier integral operators, I. *Acta Mathematica* **127**, 79–183.
- [31] Lee, J. M. (2000) *Introduction to Smooth Manifolds*, Springer, New York, USA.
- [32] Li, D., Azimi-Sadjadi, M. R. & Robinson, M. (2004) Comparison of different classification algorithms for underwater target discrimination. *IEEE Trans. Neural Networks* **15**(1), 189–194.
- [33] Li, Y., Wang, D., Ascoli, G. A., Mitra, P. P. & Wang, Y. (2017) Metrics for comparing neuronal tree shapes based on persistent homology. *PLoS ONE* **12**.
- [34] Liu, H., Runkle, P., Carin, L., Yoder, T., Giddings, T., Couchman, L. & Bucaro, J. (2004) Classification of distant targets situated near channel bottoms. *J. Acoust. Soc. Am.* **115**(3), 1185–1197.
- [35] Livingston, C. (1993) *Knot Theory*, Mathematical Association of America, Washington, DC, USA.
- [36] Luo, H., Patania, A., Kim, J. & Vejdemo-Johansson, M. (2020) Generalized penalty for circular coordinate representation, arxiv:2006.02554.
- [37] Mallat, S. (2012) Group invariant scattering. *Commun. Pure Appl. Math.* **65**(10), 1331–1398.
- [38] Marston, T. & Kennedy, J. (2021) Spatially variant autofocus for circular synthetic aperture sonar. *J. Acoust. Soc. Am.* **149**(6), 4078–4093.
- [39] Marston, T. M., Kennedy, J. L. & Marston, P. L. (2011) Coherent and semi-coherent processing of limited-aperture circular synthetic aperture (csas) data. In: *OCEANS'11 MTS/IEEE KONA*, pp. 1–6.
- [40] Marston, T. M., Kennedy, J. L. & Marston, P. L. (2014) Autofocusing circular synthetic aperture sonar imagery using phase corrections modeled as generalized cones. *J. Acoust. Soc. Am.* **136**(2), 614–622.
- [41] Oliver, C. & Quegan, S. (2004) *Understanding Synthetic Aperture Radar Images*, SciTech, Raleigh, N.C., USA.
- [42] Perea, J. A. (2018) Multiscale projective coordinates via persistent cohomology of sparse filtrations. *Discrete Comput. Geometry* **59**, 175–225.
- [43] Perea, J. A. (2020) Sparse circular coordinates via principal  $\mathbb{Z}$ -bundles. In: *Topological Data Analysis*, Springer, pp. 435–458.
- [44] Plotnick, D. S., Marston, P. L. & Marston, T. M. (2014) Fast nearfield to farfield conversion algorithm for circular synthetic aperture sonar. *J. Acoust. Soc. Am.* **136**(2), EL61–EL66.
- [45] Robinson, M. (2013) Multipath-dominant, pulsed doppler analysis of rotating blades. *IET Radar Sonar Navig.* **7**(3), 217–224.
- [46] Robinson, M. (2014) *Topological Signal Processing*, Springer, Berlin Heidelberg, Germany.
- [47] Robinson, M. (2015) Universal factorizations of quasiperiodic functions. In: *Sampling Theory and Applications (SampTA 2015)*, Washington, DC.
- [48] Robinson, M. (2016) A topological lowpass filter for quasiperiodic signals. *IEEE Signal Process. Lett.* **23**(12), 1771–1775.
- [49] Robinson, M., Dumiak, J., Fennell, S. & DiZio, V. (2018) Geometry and topology of the space of sonar target echos. *J. Acoust. Soc. Am.* **143**(3), 1630–1645.
- [50] Saito, N. & Weber, D. S. (2017) Underwater object classification using scattering transform of sonar signals. In: *Optical Engineering + Applications*.
- [51] Spivak, D. I. (2014) *Category Theory for the Sciences*, MIT Press, Cambridge, MA, USA.
- [52] Takeuchi, H. (2021) The persistent homology of a sampled map: from a viewpoint of quiver representations. *J. Appl. Comput. Topol.* **5**, 179–213.

- [53] Vejdemo-Johansson, M., Pokorny, F. T., Skraba, P. & Kragic, D. (2015) Cohomological learning of periodic motion. In: *Applicable Algebra in Engineering, Communication and Computing*, Vol. 26, pp. 5–26.
- [54] Wiatowski, T. & Bölcskei, H. (2015) Deep convolutional neural networks based on semi-discrete frames. In: *2015 IEEE International Symposium on Information Theory (ISIT)*, pp. 1212–1216.
- [55] Williams, D. P. (2019) Demystifying deep convolutional neural networks for sonar image classification. In: *4th Underwater Acoustics Conference and Exhibition (UACE2017)*, pp. 513–520.
- [56] Yao, D., Azimi-Sadjadi, M. R. & Dobeck, G. J. (1999) Adaptive feature mapping for underwater target classification. In: *International Joint Conference on Neural Networks*, Vol. 5, IEEE, pp. 3221–3224.